

000 001 002 003 004 005 JOINT DISTRIBUTION-INFORMED SHAPLEY VALUES 006 FOR SPARSE COUNTERFACTUAL EXPLANATIONS 007 008 009

010 **Anonymous authors**
011 Paper under double-blind review
012
013
014
015
016
017
018
019
020
021
022
023

ABSTRACT

024 Counterfactual explanations (CE) aim to reveal how small input changes flip
025 a model’s prediction, yet many methods modify more features than necessary,
026 reducing clarity and actionability. We introduce *COLA*, a model- and generator-
027 agnostic post-hoc framework that refines any given CE by computing a coupling
028 via optimal transport (OT) between factual and counterfactual sets and using it to
029 drive a Shapley-based attribution (*p-SHAP*) that selects a minimal set of edits while
030 preserving the target effect. Theoretically, OT minimizes an upper bound on the
031 W_1 divergence between factual and counterfactual outcomes and that, under mild
032 conditions, refined counterfactuals are guaranteed not to move farther from the
033 factuals than the originals. Empirically, across four datasets, twelve models, and
034 five CE generators, COLA achieves the same target effects with only 26–45% of the
035 original feature edits. On a small-scale benchmark, COLA shows near-optimality.

1 BACKGROUND

036 Explainable Artificial Intelligence (XAI) is key to building transparent and trustworthy AI systems
037 (Arrieta et al., 2020; Das & Rad, 2020). Feature attribution methods such as Shapley values (Sun-
038 dararajan & Najmi, 2020; Lundberg & Lee, 2017) quantify each input feature’s contribution to a
039 model, helping simplify complex decisions; in healthcare, they can highlight factors like age and
040 medical history (Ter-Minassian et al., 2023; Nohara et al., 2022). Counterfactual Explanations (CE)
041 (Wachter et al., 2017; Guidotti, 2022) instead illustrate how small input changes yield different out-
042 comes. Despite hundreds of CE algorithms (Guidotti, 2022; Verma et al., 2020), no universal solution
043 exists since objectives vary: some find a single counterfactual per instance, others handle groups or
044 datasets to generate global CEs (Rawal & Lakkaraju, 2020; Ley et al., 2022; 2023; Carrizosa et al.,
045 2024), and still others search for counterfactual distributions (You et al., 2025).
046

047 **Problem Description and Challenges** We address a general and comprehensive problem in this
048 paper, which builds on the extensive foundations established in the literature (see Appendix A). To be
049 specific, we seek to answer the following question:

050 *Given a (group of) factual instance(s), how can we devise an action plan that re-
051 quires the least feature modifications to achieve a desired counterfactual outcome?*

	\mathbf{x}	\mathbf{z}'	\mathbf{z}''	\mathbf{y}^*
	$\mathbf{\textcircled{a}}$	$\mathbf{\textcircled{b}}$	$\mathbf{\textcircled{c}}$	$\mathbf{\textcircled{d}}$
052	200	5	No	
053	250	8	Yes	
054	150	3	No	
055	350	9	Yes	
056	100	2	No	
057	150	6	No	
058				
059				
060				
061				
062				
063				
064				
065				
066				
067				
068				
069				
070				
071				
072				
073				
074				
075				
076				
077				
078				
079				
080				
081				
082				
083				
084				
085				
086				
087				
088				
089				
090				
091				
092				
093				
094				
095				
096				
097				
098				
099				
100				
101				
102				
103				
104				
105				
106				
107				
108				
109				
110				
111				
112				
113				
114				
115				
116				
117				
118				
119				
120				
121				
122				
123				
124				
125				
126				
127				
128				
129				
130				
131				
132				
133				
134				
135				
136				
137				
138				
139				
140				
141				
142				
143				
144				
145				
146				
147				
148				
149				
150				
151				
152				
153				
154				
155				
156				
157				
158				
159				
160				
161				
162				
163				
164				
165				
166				
167				
168				
169				
170				
171				
172				
173				
174				
175				
176				
177				
178				
179				
180				
181				
182				
183				
184				
185				
186				
187				
188				
189				
190				
191				
192				
193				
194				
195				
196				
197				
198				
199				
200				
201				
202				
203				
204				
205				
206				
207				
208				
209				
210				
211				
212				
213				
214				
215				
216				
217				
218				
219				
220				
221				
222				
223				
224				
225				
226				
227				
228				
229				
230				
231				
232				
233				
234				
235				
236				
237				
238				
239				
240				
241				
242				
243				
244				
245				
246				
247				
248				
249				
250				
251				
252				
253				
254				
255				
256				
257				
258				
259				
260				
261				
262				
263				
264				
265				
266				
267				
268				
269				
270				
271				
272				
273				
274				
275				
276				
277				
278				
279				
280				
281				
282				
283				
284				
285				
286				
287				
288				
289				
290				
291				
292				
293				
294				
295				
296				
297				
298				
299				
300				
301				
302				
303				
304				
305				
306				
307				
308				
309				
310				
311				
312				
313				
314				
315				
316				
317				
318				
319				
320				
321				
322				
323				
324				
325				
326				
327				
328				
329				
330				
331				
332				
333				
334				
335				
336				
337				
338				
339				
340				
341				
342				
343				
344				
345				
346				
347				
348				
349				
350				
351				
352				
353				
354				
355				
356				
357				
358				
359				
360				
361				
362				
363				
364				
365				
366				
367				
368				
369				
370				
371				
372				
373				
374				
375				
376				
377				
378				
379				
380				
381				
382				
383				
384				
385				
386				
387				
388				
389				
390				
391				
392				
393				
394				
395			</td	

054 Three major challenges remain in addressing this problem. First, it is unrealistic to expect a single CE
 055 algorithm to meet all the needs universally, as the problem is often task-specific. Second, the approach
 056 should not rely on strong assumptions about the model (for example, requiring differentiability or
 057 special structures) to ensure its applicability across a wide range of models. Third, feature attributions
 058 (FA) like feature importance can be misleading due to the lack of coherence between the FA scores and
 059 the changes for counterfactual effect. In other words, it is not effective to perform FA independently of
 060 CE to select the most important features to change. We will demonstrate later that this decoupling can
 061 result in counterproductive feature modifications (also referred to as actions from users/stakeholders)
 062 in Result II of Section 6, as the features deemed important generally may not align with the specific
 063 pathways to achieve the desired counterfactual outcomes.

064
 065 **Main Contributions** We introduce COunterfactuals with Limited Actions (COLA), a general
 066 post-hoc framework that refines CE across models and CE generators by using an optimal transport
 067 (OT)-induced coupling between factual and counterfactual sets to guide Shapley attributions. This
 068 yields p -SHAP, which unifies other commonly used Shapley methods under appropriate couplings and
 069 offers a modular interface for attribution and edit selection. We provide theoretical guarantees: OT
 070 minimizes an upper bound on the W_1 divergence, and under mild conditions refined counterfactuals
 071 are provably no farther from factuals than the originals. Empirically, across four datasets, twelve
 072 models, and five CE methods, COLA with p -SHAP achieves the same target effects with only 26–45%
 073 of the original feature edits. In a small-scale benchmark, COLA is near-optimal.
 074

075 2 PROBLEM FORMULATION

076 We formally formulate the problem described in Figure 1. Denote $f : \mathbb{R}^d \rightarrow \mathbb{R}$ as a black-box
 077 machine learning (ML) model. Denote by \mathbf{x} any observed (factual) data with n rows and d columns
 078 ($\mathbf{x} \in \mathbb{R}^{n \times d}$, $n \geq 1$, and $d \geq 1$). Let \mathbf{y}^* be the target model output ($\mathbf{y}^* \in \mathbb{R}^m$, $m \geq 1$). The
 079 optimization is to look for a (group of) counterfactual data instance(s) \mathbf{z} ($\mathbf{z} \in \mathbb{R}^{n \times d}$) subject to a
 080 maximum number of allowed feature changes, C , to achieve model output(s) as close as possible to
 081 \mathbf{y}^* . Let D denote a divergence function that measures the dissimilarity between two entities. The
 082 problem is below.
 083

$$\min_{\mathbf{c}, \mathbf{z}} D(f(\mathbf{z}), \mathbf{y}^*) \quad (1a)$$

$$\text{s.t. } D(\mathbf{z}, \mathbf{x}) \leq \epsilon \quad (1b)$$

$$\sum_{i=1}^n \sum_{k=1}^d c_{ik} \leq C \quad (1c)$$

$$z_{ik} \leq x_{ik}(1 - c_{ik}) + M c_{ik} \quad i = 1, \dots, n, k = 1, \dots, d \quad (1d)$$

$$z_{ik} \geq x_{ik}(1 - c_{ik}) - M c_{ik} \quad i = 1, \dots, n, k = 1, \dots, d \quad (1e)$$

093 The objective equation 1a and the constraint equation 1b formulate the typical CE optimization.
 094 Namely, \mathbf{z} is expected to make $f(\mathbf{z})$ close to \mathbf{y}^* yet stays close to \mathbf{x} . Then \mathbf{z} can be used as a
 095 counterpart reference to explain why $f(\mathbf{x})$ does not achieve \mathbf{y}^* . We do not limit the function D to
 096 any specific type of divergence function, allowing it to stay general. Example functions of D can be
 097 Euclidean distance, OT, maximum mean discrepancy (MMD), or differences of the model outcome
 098 in mean or median. Then, equation 1c–equation 1e compose the CE optimization constrained by
 099 actions. On top of the counterfactual data \mathbf{z} , we also optimize an indicator variable \mathbf{c} , such that z_{ik}
 100 is not allowed to change iff $c_{ik} = 0$. Maximum C changes are allowed as imposed by equation 1c.
 101 Inspecting equation 1d and equation 1e, if $c_{ik} = 0$, x_{ik} equals z_{ik} and no changes happen at (i, k) .
 102 Otherwise, if $c_{ik} = 1$, remark that M is a sufficiently large constant such that z_{ik} has good freedom
 103 to change.

104 To solve equation 1, we resort to FA to identify the most influential features to obtain the modification
 105 indicator variable \mathbf{c} . The next section introduces commonly used Shapley value methods for FA,
 106 which, together with our later proposed one, are integrated into our algorithmic framework COLA, to
 107 obtain the refined counterfactual \mathbf{z} . The problem is computationally difficult even when $d = 1$ for
 linear models, see Appendix B.

108 **3 PRELIMINARIES ON SHAPLEY VALUE**
 109

110 We briefly review Shapley value methods for feature attribution (FA), which serve as baselines within
 111 our framework COLA. A coalitional game is defined by a set of players (features) $\mathcal{F} = \{1, \dots, d\}$
 112 and a characteristic function $v : 2^{\mathcal{F}} \rightarrow \mathbb{R}$ with $v(\emptyset) = 0$. For a player k and coalition S , the marginal
 113 contribution is

$$\Delta(k, S) = v(S \cup k) - v(S). \quad (2)$$

114 The Shapley value is then

$$\phi_k = \frac{1}{d} \sum_{S \subset \mathcal{F} \setminus \{k\}} \binom{d-1}{|S|}^{-1} \Delta(k, S), \quad (3)$$

115 which averages $\Delta(k, S)$ across all subsets, providing a fair distribution of $v(\mathcal{F})$ among features
 116 (Sundararajan & Najmi, 2020). For a data point \mathbf{x}_i , $\mathbf{x}_{i,S}$ denotes its restriction to S .

117 We next outline three common instantiations. *Baseline Shapley (B-SHAP)* uses a fixed reference \mathbf{r}_j :

$$v_B^{(i)}(S) = f(\mathbf{x}_{i,S}; \mathbf{r}_j, \mathcal{F} \setminus S) - f(\mathbf{r}_j), \quad (4)$$

118 assuming exact alignment between \mathbf{x} and \mathbf{r} (Lundberg & Lee, 2017; Sun & Sundararajan, 2011;
 119 Merrick & Taly, 2020). *Random Baseline Shapley (RB-SHAP)* replaces the baseline with a random
 120 draw from a background distribution \mathcal{D} (often the training set):

$$v_{RB}^{(i)}(S) = \mathbb{E}_{\mathbf{x}' \sim \mathcal{D}}[f(\mathbf{x}_{i,S}; \mathbf{x}'_{\mathcal{F} \setminus S})] - \mathbb{E}_{\mathbf{x}' \sim \mathcal{D}}[f(\mathbf{x}')], \quad (5)$$

121 as in (Lundberg & Lee, 2017; Merrick & Taly, 2020). *Counterfactual Shapley (CF-SHAP)* further
 122 sets \mathcal{D} to the counterfactual distribution conditioned on \mathbf{x}_i :

$$v_{CF}^{(i)}(S) = \mathbb{E}_{\mathbf{r} \sim \mathcal{D}(\mathbf{x}_i)}[f(\mathbf{x}_{i,S}; \mathbf{r}_{\mathcal{F} \setminus S})] - \mathbb{E}_{\mathbf{r} \sim \mathcal{D}(\mathbf{x}_i)}[f(\mathbf{r})], \quad (6)$$

123 which assumes a probabilistic alignment and has shown advantages for contrastive attribution (Albini
 124 et al., 2022; Kommiya Mothilal et al., 2021).

125 **4 THE PROPOSED JOINT-PROBABILITY-INFORMED SHAPLEY (*p*-SHAP) AND
 126 ITS THEORETICAL ASPECTS**

127 **(Proposed) *p*-SHAP** We generalize equation 4–equation 6 by integrating an algorithm A_{Prob} that
 128 returns their joint probability.¹ Our *p*-SHAP is defined as follows.

$$v^{(i)}(S) = \mathbb{E}_{\mathbf{r} \sim p(\mathbf{r} | \mathbf{x}_i)}[f(\mathbf{x}_{i,S}; \mathbf{r}_{\mathcal{F} \setminus S})] - \mathbb{E}_{\mathbf{r} \sim p(\mathbf{r})}[f(\mathbf{r})] \quad (7a)$$

$$\text{s.t. } p = A_{\text{Prob}}(\mathbf{x}, \mathbf{r}) \quad (7b)$$

129 Crucially, unlike prior methods that rely on random baselines, *p*-SHAP solves the alignment problem
 130 by identifying the optimal coupling via OT. This reformulates feature attribution not merely as a
 131 prediction decomposition, but as a transport problem that minimizes the cost of explanation.

132 Remark that A_{Prob} is independent of the CE algorithm, but only depends on the generated counterfactual \mathbf{r} . By focusing solely on these fixed components, *p*-SHAP ensures consistency in FA without
 133 being influenced by the variability of different CE generation processes, which is a major difference
 134 to CF-SHAP. Contrary to common expectations, we demonstrate that OT can be more effective than
 135 relying on a counterfactual distribution defined by a CE generation mechanism as done by Albini
 136 et al. (2022), in Result II of Section 6 later.

137 Especially, one of the focus in this paper is to consider the OT problem (also the 2-Wasserstein
 138 divergence) defined below. And the transportation plan \mathbf{p}_{OT} obtained by solving OT is used as the
 139 joint distribution of \mathbf{x} and \mathbf{r} in *p*-SHAP.

$$\mathbf{p}_{\text{OT}} = \arg \min_{\mathbf{p} \in \Pi(\mu, \nu)} \sum_{i=1}^n \sum_{j=1}^m p_{ij} \|\mathbf{x}_i - \mathbf{r}_j\|_2^2 + \varepsilon \sum_{i=1}^n \sum_{j=1}^m p_{ij} \log \left(\frac{p_{ij}}{\mu_i \nu_j} \right). \quad (8)$$

140 ¹First, *p*-SHAP degrades to B-SHAP in equation 4 when A_{Prob} defines a joint distribution between \mathbf{x} and
 141 \mathbf{r} that indicates an $i \leftrightarrow j$ alignment of for any $\mathbf{x}_i, \mathbf{r}_j$. Second, *p*-SHAP degrades to RB-SHAP in equation 5
 142 when A_{Prob} is defined to be independent of CE and associates with an arbitrary distribution \mathcal{D} . Third, *p*-SHAP
 143 degrades to CF-SHAP in equation 6 when A_{Prob} is built upon a known distribution of CE.

162 Note that μ and ν represent the marginal distributions of \mathbf{x} and \mathbf{r} respectively, and $\Pi(\mu, \nu)$ the set
 163 of joint distributions (i.e. all possible transport plans). The term $\varepsilon \sum_{i=1}^n \sum_{j=1}^m p_{ij} \log(p_{ij}/(\mu_i \nu_j))$
 164 is the entropic regularization with $\varepsilon \geq 0$ being the coefficient. Such regularization ($\varepsilon > 0$) helps
 165 accelerate the computation of OT.
 166

167 **Theoretical Aspects of p -SHAP** OT minimizes the total feature modification cost (i.e. modifying
 168 \mathbf{x} towards \mathbf{r}) under its obtained alignment between factual \mathbf{x} and counterfactual \mathbf{r} . This directly
 169 corresponds to our objective of finding feature modifications that achieve the counterfactual outcomes
 170 at minimal cost. We can further strengthen this connection theoretically under the Lipschitz continuity
 171 assumption of the predictive model f . In Theorem 4.1 below (proof in Appendix C), we establish
 172 that the transportation plan \mathbf{p}_{OT} used in p -SHAP is effective in minimizing an upper bound on the
 173 divergence between $f(\mathbf{x})$ and \mathbf{y}^* . Specifically, the 1-Wasserstein distance between $f(\mathbf{x})$ and \mathbf{y}^* , is
 174 bounded by the Lipschitz constant (assuming Lipschitz continuity of f) multiplied by the square
 175 root of the minimized expected cost of changing \mathbf{x} towards \mathbf{r} , i.e. $\sum_{i,j} p_{ij} \|\mathbf{x}_i - \mathbf{r}_j\|_2^2$ where p_{ij}
 176 ($j = 1, 2, \dots, m$) quantify how the feature values of \mathbf{x}_i should be adjusted towards those of one or
 177 multiple \mathbf{r}_j . Practically, this means that in p -SHAP, the OT plan \mathbf{p}_{OT} provides a strategy to adjust
 178 the feature values of \mathbf{x} towards those of \mathbf{r} in a way that minimizes the expected modification cost
 179 $\sum_{i,j} p_{ij} \|\mathbf{x}_i - \mathbf{r}_j\|_2^2$. Compared to other modification plans ($\mathbf{p} \in \Pi$), \mathbf{p}_{OT} yields the minimal possible
 180 cost, which in turn provides the tightest upper bound on the violation of the counterfactual effect
 181 $W_1(f(\mathbf{x}), \mathbf{y}^*)$ in proportion to this cost.

182 **Theorem 4.1** (p -SHAP Towards Counterfactual Effect). *Consider the 1-Wasserstein divergence W_1 ,
 183 i.e. $W_1(f(\mathbf{x}), \mathbf{y}^*) = \min_{\mathbf{p} \in \Pi} \sum_{i=1}^n \sum_{j=1}^m \pi_{ij} |f(\mathbf{x}_i) - \mathbf{y}_j^*|$. Suppose the counterfactual outcome
 184 \mathbf{y}^* is fully achieved by \mathbf{r} , i.e. $\mathbf{y}_j^* = f(\mathbf{r}_j)$ ($j = 1, 2, \dots, m$). Assume that the model $f : \mathbb{R}^d \rightarrow \mathbb{R}$ is
 185 Lipschitz continuous with Lipschitz constant L . The expected absolute difference in model outputs
 186 between the factual and counterfactual instances, weighted by \mathbf{p}_{OT} (with $\varepsilon = 0$), is bounded by:*

$$187 \quad W_1(f(\mathbf{x}), \mathbf{y}^*) \leq L \sqrt{\sum_{i=1}^n \sum_{j=1}^m p_{ij}^{OT} \|\mathbf{x}_i - \mathbf{r}_j\|_2^2} \leq L \sqrt{\sum_{i=1}^n \sum_{j=1}^m p_{ij} \|\mathbf{x}_i - \mathbf{r}_j\|_2^2} \quad \forall \mathbf{p} \in \Pi.$$

190 *Namely, \mathbf{p}_{OT} minimizes the upper bound of $W_1(f(\mathbf{x}), \mathbf{y}^*)$, where the upper bound is based on the
 191 expected feature modification cost.*

192 *Although Theorem 4.1 bounds the transport cost, it serves as a convex proxy for the \mathcal{NP} -hard
 193 discrete sparsity (L_0) problem. By concentrating attribution mass on the most efficient paths, the OT
 194 coupling effectively guides the greedy selection in Algorithm 1 to discard non-essential features. In
 195 addition, p -SHAP is conceptually correct in attributing the causal behavior to the modifications of the
 196 characteristics, stated in Theorem 4.2 below (proof in Appendix D).*

197 **Theorem 4.2** (Interventional Effect of p -SHAP). *For any subset $S \subseteq \mathcal{F}$ and any \mathbf{x}_i ($i = 1, 2, \dots, n$),
 198 $v^{(i)}(S)$ represents the causal effect of the difference between the expected value of $f(\mathbf{r})$ under the
 199 intervention on features S and the unconditional expected value of $f(\mathbf{r})$. Mathematically, this is
 200 expressed as:*

$$201 \quad \mathbb{E}[f(\mathbf{r})] + v^{(i)}(S) = \mathbb{E}[f(\mathbf{r}) | do(\mathbf{r}_S = \mathbf{x}_{i,S})].$$

204 Furthermore, we remark that p -SHAP preserves nice axioms of B-SHAP and RB-SHAP, which makes
 205 it an effective tool for attributing features. We omit the proof but refer to (Sundararajan & Najmi,
 206 2020; Lundberg & Lee, 2017) as a reference for axioms of Shapley.

208 5 THE ALGORITHMIC FRAMEWORK COLA

210 **Sketch** The algorithmic framework COLA, stated in Algorithm 1 below, aims to solve equation 1
 211 and is established on four categories of algorithms. We explain Algorithm 1 in details below, along
 212 with an illustration in Figure 2.

214 **Line 1** (*Applying a CE algorithm to find a counterfactual \mathbf{r}*). The CE algorithm A_{CE} takes the
 215 model f , the factual \mathbf{x} , the target outcome \mathbf{y}^* , and the tolerance ϵ as input. The algorithm returns a
 216 counterfactual \mathbf{r} staying close with \mathbf{x} , with $\mathbf{y}^* = f(\mathbf{r})$ and $D(\mathbf{r}, \mathbf{x}) \leq \epsilon$.

216 **Algorithm 1** CCounterfactuals with Limited Actions (COLA)
217
218 **Require:** Model f , factual $\mathbf{x} \in \mathbb{R}^{n \times d}$, target $\mathbf{y}^* \in \mathbb{R}^m$, ϵ , and C
219 **Ensure:** Action plan $\mathbf{c} \in \mathbb{R}^{n \times d}$ and correspondingly a refined counterfactual $\mathbf{z} \in \mathbb{R}^{n \times d}$
220 1: Use $A_{CE}(f, \mathbf{x}, \mathbf{y}^*, \epsilon)$ to obtain $\mathbf{r} \in \mathbb{R}^{m \times d}$, with $\mathbf{y}^* = f(\mathbf{r})$ and $D(\mathbf{r}, \mathbf{x}) \leq \epsilon$.
221 2: Use $A_{Prob}(\mathbf{x}, \mathbf{r})$ to obtain the joint distribution matrix $\mathbf{p} \in \mathbb{R}_+^{n \times m}$.
222 3: Use $A_{Shap}(\mathbf{x}, \mathbf{r}, \mathbf{p})$ to obtain the shapley values $\phi \in \mathbb{R}^{n \times d}$ for each element of \mathbf{x} .
223 4: Normalize the element-wise absolute values of ϕ , i.e., $\varphi_{ik} \leftarrow |\phi_{ik}| / \|\phi\|_1$ ($\varphi \in \mathbb{R}_+^{n \times d}$).
224 5: Use $A_{Value}(\mathbf{r}, \mathbf{p})$ to obtain matrix $\mathbf{q} \in \mathbb{R}^{n \times d}$.
225 6: For $\mathbf{c} \in \{0, 1\}^{n \times d}$, $c_{ik} \leftarrow 0$ ($i = 1 \dots n$, $k = 1, \dots d$).
226 7: Sample C pairs (i, k) according to the probability matrix φ , and let $c_{ik} = 1$ for them.
227 8: Let $\mathbf{z} \leftarrow \mathbf{x}$ ($\mathbf{z} \in \mathbb{R}^{n \times d}$).
228 9: **for** $i \leftarrow 1$ to n **do**
229 10: **for** $k \leftarrow 1$ to d **do**
230 11: **if** $c_{ik} = 1$ **then**
231 12: $z_{ik} \leftarrow q_{ik}$
232 13: **end if**
233 14: **end for**
234 15: **end for**
235 16: **return** \mathbf{c} and \mathbf{z}

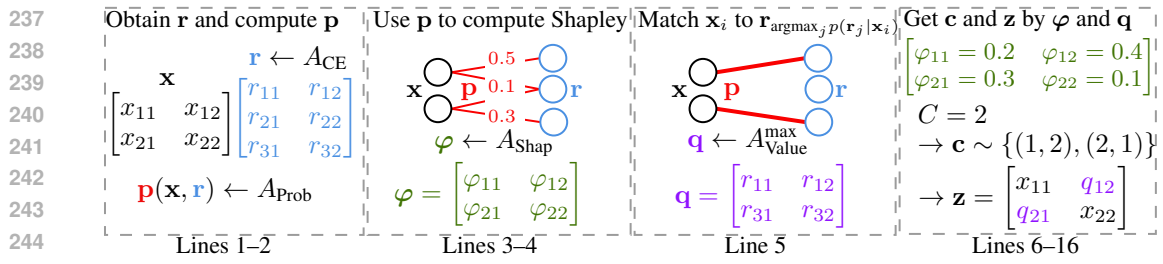


Figure 2: [An illustration of COLA] This figure shows how COLA gets \mathbf{c} and \mathbf{z} for equation 1. We use A_{Value}^{\max} for illustration in line 5 due to its simplicity. In lines 6–16, we assume $C = 2$, and the sampling yields exactly two positions for modifications according to the probability matrix φ .

252 **Line 2 (Seeking a joint distribution of \mathbf{x} and \mathbf{r}).** We use an algorithm A_{Prob} for this task, which
253 takes \mathbf{x} and \mathbf{r} as input, and outputs a matrix representing the joint distribution of all n and m data
254 points in \mathbf{x} and \mathbf{r} , respectively. The joint distribution \mathbf{p} represents an alignment relationship (or
255 matching) between the factual rows and counterfactual rows, and we use it in Line 5 to compute
256 the values that can be used for composing \mathbf{z} later on. As discussed in Section 3, A_{Prob} can be based
257 on OT to compute a joint distribution that yields the smallest OT distance between \mathbf{x} and \mathbf{r} , if the
258 alignment relationship between their rows are unknown. Otherwise, it is recommended to select a
259 joint distribution that accurately reflects the alignment between the rows in \mathbf{x} and \mathbf{r} .

260 **Lines 3–4 (p-SHAP FA).** We apply equation 7 to compute the shapley value for \mathbf{x} . The joint distribution
261 \mathbf{p} can be used here (without being forced) to properly align each row of \mathbf{x} with its corresponding
262 counterfactual rows of \mathbf{r} , such that the selected rows in \mathbf{r} serve as the most representative contrastive
263 reference for the row in \mathbf{x} . Numerically, this alignment significantly influences our contrastive FA.
264 Then, the shapley values (as a matrix) of \mathbf{x} is taken element-wisely with the absolute values and
265 normalized (such that all values sum up to one). The resulted matrix φ forms our FA.

266 **Line 5 (Computing feature values).** The algorithm A_{Value} is used for this task, which takes the
267 counterfactual \mathbf{r} and the joint distribution \mathbf{p} as input. For any row i in \mathbf{x} , A_{Value} selects one or multiple
268 row(s) in \mathbf{r} , used as references for making changes in \mathbf{x} . The algorithm returns a matrix $\mathbf{q} \in \mathbb{R}^{n \times d}$,
269 where each element q_{ik} serves as a counterfactual candidate for x_{ik} ($\forall i, k$). Below, we introduce
 A_{Value}^{\max} and A_{Value}^{avg} , respectively for the cases of selecting single row and selecting multiple rows.

270 For any row \mathbf{x}_i , A_{Value}^{\max} selects the row of \mathbf{r} with the highest probability.
 271

$$272 \mathbf{q} = A_{\text{Value}}^{\max}(\mathbf{r}, \mathbf{p}) \text{ where } q_{ik} = r_{\tau(i),k} \text{ and } \tau(i) = \arg \max_{j=1,2,\dots,m} p_{ij}. \quad (9)$$

274 The algorithm A^{avg} computes q_{ik} as a convex combination as a weighted average of $r_{1k}, r_{2k}, \dots, r_{mk}$.
 275

$$276 \mathbf{q} = A_{\text{Value}}^{\text{avg}}(\mathbf{r}, \mathbf{p}) \text{ where } q_{ik} = \sum_{j=1}^m \left(\frac{p_{ij}}{\sum_{j'=1}^m p_{ij'}} \right) r_{jk}. \quad (10)$$

279 **Lines 6–16.** Recall that the non-negative matrix φ is normalized to have its summation being one.
 280 We could hence treat it as a policy to select the positions in \mathbf{x} for value replacement (i.e. $c_{ik} = 1$), as
 281 what line 7 does. Then, for any i and k with $c_{ik} = 1$, x_{ik} gets modified to q_{ik} , and the modified matrix
 282 is then returned as \mathbf{z} together with \mathbf{c} forming the optimized solutions of the problem in equation 1.
 283

284 By Theorem 4.1, COLA is designed to minimize the dissimilarity between $f(\mathbf{z})$ and \mathbf{y}^* by modifying
 285 \mathbf{z} based on feature attribution results, which identify the most important features to adjust to achieve
 286 the desired counterfactual effect. The theorem below (proof in Appendix E) demonstrates that the
 287 refined \mathbf{z} , produced by the COLA framework, satisfies the constraint equation 1b in the typical
 288 scenario where $n = m$, using the Frobenius norm as the distance measure. Empirical evidence
 289 supporting the general applicability of this conclusion can be found in Table 3.
 290

291 **Theorem 5.1** (Counterfactual Proximity). *Let $\mathbf{q} \in \mathbb{R}^{n \times d}$ be the aligned reference matrix derived
 292 from the counterfactual set $\mathbf{r} \in \mathbb{R}^{m \times d}$ via the value assignment step $\mathbf{q} = A_{\text{Value}}(\mathbf{r}, \mathbf{p})$, where \mathbf{p} is
 293 the coupling matrix. For any dimensions $n, m \geq 1$, the refined counterfactual \mathbf{z} constructed by the
 294 COLA framework satisfies:*

$$295 \|\mathbf{z} - \mathbf{x}\|_F \leq \|\mathbf{q} - \mathbf{x}\|_F.$$

296 *This inequality guarantees that the refined counterfactual \mathbf{z} is strictly closer (or equal) to the factual
 297 input \mathbf{x} compared to the aligned counterfactual proposal \mathbf{q} , ensuring that the refinement process
 298 introduces no additional divergence.*

299 **Corollary 5.2.** *In the special case where $n = m$ and the OT plan \mathbf{p} corresponds to a deterministic
 300 permutation σ (i.e., obtained without entropic regularization, $\varepsilon = 0$), the matrix \mathbf{q} becomes a
 301 row-permuted version of \mathbf{r} (denoted as \mathbf{r}_σ , where $q_i = r_{\sigma(i)}$). In this setting, the bound simplifies to:*

$$302 \|\mathbf{z} - \mathbf{x}\|_F \leq \|\mathbf{r}_\sigma - \mathbf{x}\|_F,$$

303 *recovering the intuition that the refined counterfactual is at least as close to the factuals as the
 304 original counterfactual set reordered by σ .*

305 **Complexity of COLA** Let $O(M_{\text{CE}})$ be the algorithm complexity of A_{CE} . For algorithm A_{Shap} ,
 306 consider using weighted linear regression to estimate Shapley values, and denote by M_{Shap} the number
 307 of sampled subsets. The complexity of COLA with respect to n, m, d , and the regularization parameter
 308 ε of entropic OT is $O(M_{\text{CE}}) + O(nm \log(1/\varepsilon)) + O(ndM_{\text{Shap}}) + N$ where $N = O(nm) + O(nd)$
 309 if A_{Value}^{\max} is used and $N = O(nmd)$ if $A_{\text{Value}}^{\text{avg}}$ is used. See Appendix F.
 310

311 6 NUMERICAL RESULTS

312 This section evaluates the effectiveness of COLA in addressing the problem in equation 1, with
 313 $\mathbf{y}^* = f(\mathbf{r})$ where \mathbf{r} is the counterfactual obtained from a CE method A_{CE} . We adopt four different
 314 divergence functions: OT evaluates the distance between entire distributions. MMD evaluates the
 315 divergence between the means of two distributions in a high-dimensional feature space. The absolute
 316 mean difference (MeanD) and absolute median difference (MedianD) evaluate the divergence between
 317 mean and median, respectively. The numerical results aim at showing: I) *COLA’s effectiveness for
 318 modification minimality*. II) *p-SHAP’s superior performance than other Shapley methods towards
 319 modification minimality*. III) *COLA’s near-optimal performance*.
 320

321 **Experiment Setup** The experiments² are conducted with 4 datasets for binary classification tasks,
 322 5 CE algorithms that are designed for diverse goals, and 12 classifiers, shown in Table 1, where a
 323 combination of dataset, A_{CE} algorithm, and a model defines an “experiment scenario”.

324 Table 1: [Experiment Scenarios Setup] Four datasets are used to benchmark five CE algorithms over
 325 12 models. A “scenario” is defined to be a combination of dataset, A_{CE} algorithm, and a model f .
 326

Dataset	HELOC (FICO, 2018), German Credit (Hofmann, 1994), Hotel Bookings (Antonio et al., 2019), COMPAS (Jeff Larson et al., 2016)
A_{CE}	DiCE (Mothilal et al., 2020), AReS (Rawal & Lakkaraju, 2020), GlobeCE (Ley et al., 2023), KNN (Albini et al., 2022; Contardo et al.; Forel et al., 2023), Discount (You et al., 2025)
Model f	Bagging, LightGBM, Support Vector Machine (SVM), Gaussian Process (GP), Radial Basis Function Network (RBF), XGBoost, Deep Neural Network (DNN), Random Forest (RndForest), AdaBoost, Gradient Boosting (GradBoost), Logistic Regression (LR), Quadratic Discriminant Analysis (QDA)

337 Table 2: [Experiment Methods Setup] The table defines 6 methods for comparisons, colored to align
 338 with Figure 3. Each method is put in an experiment scenario, as defined in Table 1, for benchmarking.
 339

Method	The probability \mathbf{p} used by A_{Value} and A_{Shap}	The Shapley algorithm A_{Shap}
RB-p_{Uni}	$\mathbf{p} \leftarrow A_{Prob} : p_{ij} = 1/nm \ (\forall i, j)$	RB-SHAP, \mathcal{D} = trainset of f
RB-p_{OT}	$\mathbf{p} \leftarrow A_{Prob} : \text{Eq. equation 8}$ (but not used in A_{Shap})	RB-SHAP, \mathcal{D} = trainset of f
CF-p_{Uni}	$\mathbf{p} \leftarrow A_{Prob} : p_{ij} = 1/nm \ (\forall i, j)$	CF-SHAP, $\mathcal{D}(\mathbf{x}_i) = \mathbf{p}_i$
CF-p_{Rnd}	$\mathbf{p} \leftarrow A_{Prob} : \text{Any } \mathbf{x}_i \text{ matched randomly to an } \mathbf{r}_j$	CF-SHAP, $\mathcal{D}(\mathbf{x}_i) = \mathbf{p}_i$
CF-p_{OT}	$\mathbf{p} \leftarrow A_{Prob} : \text{Eq. equation 8}$	p -SHAP with \mathbf{p}
CF-p_{Ect}	$\mathbf{p} \leftarrow A_{Prob} : \text{Any } \mathbf{x}_i \text{ matched to known counterpart } \mathbf{r}_j$	(CF or B)-SHAP, $\mathcal{D}(\mathbf{x}_i) \rightarrow \mathbf{r}_j$

340
 341
 342
 343
 344
 345
 346
 347
 348
 349 We briefly introduce the many A_{CE} in Table 1. DiCE and KNN are data-instance-based CE methods,
 350 which yield counterfactual(s) respectively for each factual instance. AReS and GlobeCE are group-
 351 based CE methods, which find a collection of counterfactual instances for the whole factual data as a
 352 group. The algorithm Discount treats the factual instances as an empirical distribution and seeks a
 353 counterfactual distribution that stays in proximity to it.
 354

355 Table 2 defines 6 methods, where CF- p_{OT} is the proposed p -SHAP and the others are baselines. Each
 356 is put in many experiment scenarios in Table 1, benchmarked comprehensively. Each method is
 357 determined by a combination of the three algorithms A_{Prob} , A_{Value} , and A_{Shap} . For example, the first
 358 row RB- p_{Uni} uses uniform distribution as the algorithm A_{Prob} to compute \mathbf{p} , and then the computed \mathbf{p}
 359 is sequentially used in equation 9 or equation 10 of A_{Value} for computing \mathbf{q} , and A_{Shap} is RB-SHAP.
 360

361 These methods are carefully designed for ablation studies. First, RB- p_{Uni} differs with CF- p_{Uni} in
 362 that the latter uses CE information whereas the former does not. Second, CF- p_{Uni} , CF- p_{Rnd} , and
 363 CF- p_{OT} use CE in FA with different joint distributions, and we demonstrate later that the distribution
 364 computed by OT outperforms the others significantly. Third, we want to make sure that OT is useful
 365 because it informs A_{Shap} with respect to the factual-counterfactual alignment, not because of other
 366 factors, and hence a comparison of CF- p_{OT} that uses such an alignment to RB- p_{OT} that does not.
 367 Finally, CF- p_{Ect} represents a special case that each counterfactual originates from a known source,
 368 which is used as an exact factual-counterfactual alignment, making CF-SHAP also B-SHAP.
 369

370 **Result I: COLA achieves significant action reduction with a minor loss in counterfactual effect**
 371 In Table 3, we set a goal for \mathbf{z} such that $f(\mathbf{z})$ reaches 80% or 100% counterfactual effect of $f(\mathbf{r})$ ³.
 372 Observe that COLA is effective in achieving this goal, requiring significantly fewer actions in \mathbf{z} (i.e.,
 373 modifications of features in \mathbf{z}), compared to the original CE \mathbf{r} . Using COLA, one could expect to
 374 only resort to 13%–25% of the feature changes (calculated by $\|\mathbf{z} - \mathbf{x}\|/\|\mathbf{r} - \mathbf{x}\|$) to achieve the
 375 counterfactual effect of 80%. In particular, only COLA with p -SHAP (that is, CF- p_{OT}) can reach the
 376

²The code is available on both 

377 <https://anonymous.4open.science/r/Contrastive-Feature-Attribution-DFB1> and
 the submitted supplementary files.

378 ³Note that by definition, we have $D(f(\mathbf{r}), \mathbf{y}^*) = 0$, which represents a 100% counterfactual effect since
 379 $\mathbf{y}^* = f(\mathbf{r})$. To define a counterfactual effect 80%, consider the proportion of divergence reduced by the refined
 380 CE \mathbf{z} . That is, $\text{Counterfactual Effect} = 1 - D(f(\mathbf{z}), \mathbf{y}^*)/D(f(\mathbf{x}), \mathbf{y}^*) = 80\%$, with D being OT.

378
 379 Table 3: [COLA for Modification Minimality] This table shows the number of modified features in \mathbf{z}
 380 by each method, when $f(\mathbf{z})$ reaches 80% counterfactual effect of $f(\mathbf{r})$. The result of each method is
 381 averaged by running in 4 randomly selected scenarios in Table 1, with 100 runs in each scenario. The
 382 symbol “-” means the target counterfactual effect cannot be achieved.

Dataset	Method	80% Counterfactual Effect		100% Counterfactual Effect	
		# Modified Features	$\frac{\ \mathbf{z}-\mathbf{x}\ }{\ \mathbf{r}-\mathbf{x}\ }$	# Modified Features	$\frac{\ \mathbf{z}-\mathbf{x}\ }{\ \mathbf{r}-\mathbf{x}\ }$
German Credit $ \mathcal{F} = 9$	RB-p_{Uni}	—	—	—	—
	RB-p_{OT}	5.29(± 0.09)	75.9%	—	—
	CF-p_{Uni}	—	—	—	—
	CF-p_{Rnd}	—	—	—	—
	CF-p_{OT}	1.70(± 0.02)	24.3%	3.13(± 0.03)	44.9%
Hotel Bookings $ \mathcal{F} = 29$	RB-p_{Uni}	7.10(± 0.08)	24.5%	—	—
	RB-p_{OT}	8.55(± 0.08)	50.2%	—	—
	CF-p_{Uni}	7.01(± 0.07)	41.1%	—	—
	CF-p_{Rnd}	10.63(± 0.08)	62.4%	—	—
	CF-p_{OT}	2.50(± 0.03)	14.6%	4.44(± 0.02)	26.0%
COMPAS $ \mathcal{F} = 15$	RB-p_{Uni}	5.02(± 0.05)	82.7%	—	—
	RB-p_{OT}	—	—	—	—
	CF-p_{Uni}	2.80(± 0.04)	34.4%	—	—
	CF-p_{Rnd}	2.58(± 0.04)	32.1%	—	—
	CF-p_{OT}	1.25(± 0.03)	14.8%	2.45(± 0.03)	30.0%
HELOC $ \mathcal{F} = 23$	RB-p_{Uni}	—	—	—	—
	RB-p_{OT}	—	—	—	—
	CF-p_{Uni}	—	—	—	—
	CF-p_{Rnd}	2.73(± 0.04)	15.7%	—	—
	CF-p_{OT}	2.35(± 0.03)	13.4%	7.745(± 0.05)	44.7%

405 goal of the counterfactual effect of 100%, with only 26%–45% of the feature changes in original \mathbf{r} .
 406 Especially, p -SHAP leads to the best actional minimality, which is analyzed in details below.
 407

408 **Result II: p -SHAP outperforms the other Shapley methods in achieving counterfactual effect**
 409 We provide the evaluation of different Shapley methods in equation 4–equation 7 in Figure 3, where
 410 the x-axis is the number of allowed feature changes C and the y-axis is the term $D(f(\mathbf{z}), \mathbf{y}^*)$ in
 411 equation 1. First, RB- p_{Uni} and RB- p_{OT} perform significantly worse than the others, indicating the
 412 importance of using CE information in attributing features towards modification minimality in CE.
 413 Second, the result showing that CF- p_{OT} outperforms RB- p_{OT} demonstrates that the use of OT enhances
 414 the performance of p -SHAP specifically by providing effective factual-counterfactual alignment,
 415 rather than being influenced by other factors, due to that they only differ in A_{Shap} (see Table 2). Third,
 416 p -SHAP significantly outperforms CF- p_{Uni} and CF- p_{Rnd} . This shows the effectiveness of the joint
 417 distribution obtained in OT in using p -SHAP. Namely, merely using the counterfactual information
 418 for FA (as done by CF- p_{Uni} and CF- p_{Rnd}) is not enough, and a proper alignment (which does not
 419 necessarily mean the one defined by the exact counterfactual generation mechanism, as revealed in
 420 Figure 4 later) between factual and counterfactual must be considered.

421 We observed that COLA with p -SHAP possess good performance for many of the experiment
 422 scenarios defined in Table 1, as shown in Figure 3 as well as Table 3. A massive amount of such
 423 results are further demonstrated in Appendix H. In conclusion, p -SHAP outperforms all the other
 424 Shapley methods for the sparsity in CE.

425 **Result III: COLA is competitive with the mixed integer linear programming (MILP) optimum**
 426 **on tractable benchmarks** This result demonstrates the effectiveness of p -SHAP in eliminating
 427 the influence of the CE generation process by replacing the CE algorithm-dependent knowledge⁴
 428 of \mathcal{D} with the OT joint distribution between the factual and counterfactual data, shown in Figure 4.
 429 We benchmark the method CF- p_{Ect} using COLA, and focus on solving equation 1 with MeanD as

430
 431 ⁴This knowledge, i.e. exact alignment between factual and counterfactual, is available only by DiCE and
 432 KNN among all CE methods considered.

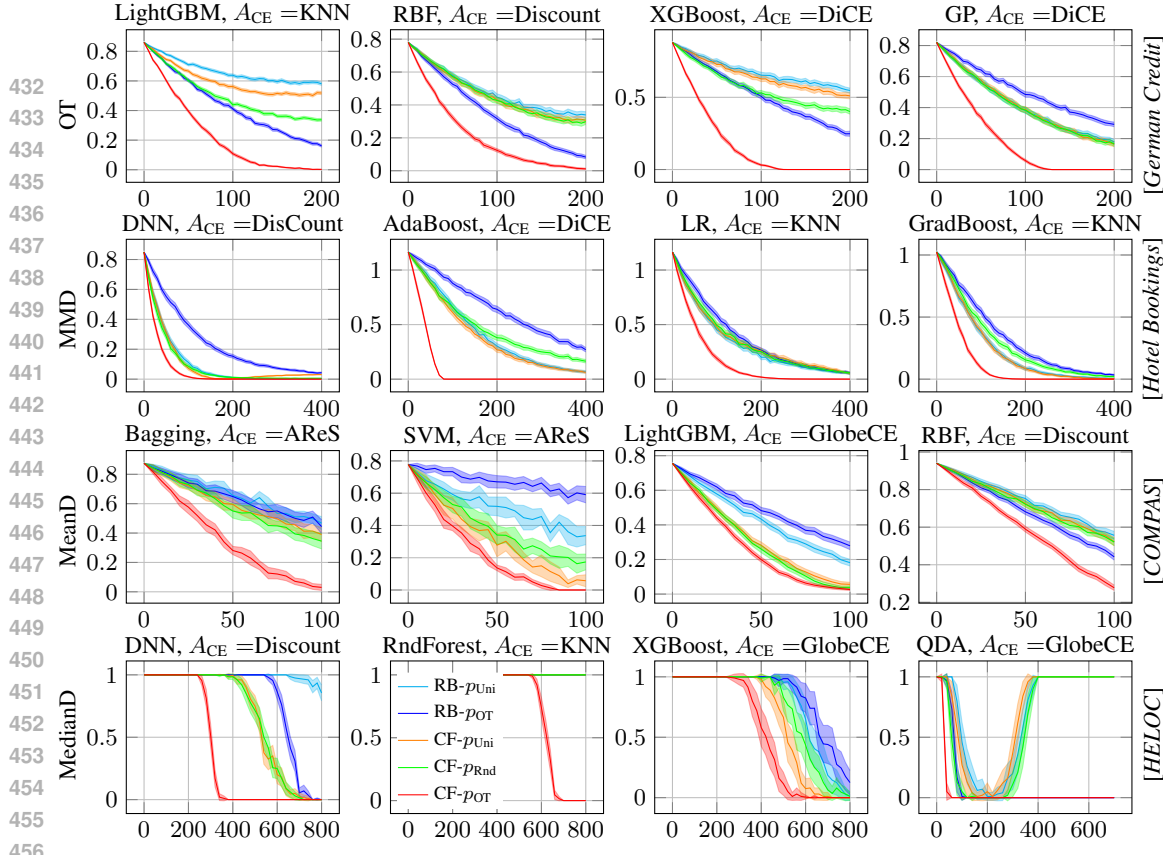


Figure 3: $D(f(\mathbf{z}), \mathbf{y}^*)$ vs. allowed actions C . Experiments are with 100 runs. The shadows show the 99.9% confidence intervals. $A_{\text{Value}}^{\text{avg}}$ is used for *HELOC* and *COMPAS*, and $A_{\text{Value}}^{\text{max}}$ is used for *German Credit* and *Hotel Bookings*. The legend inside “RndForest, $A_{\text{CE}} = \text{KNN}$ ” applies to all plots.

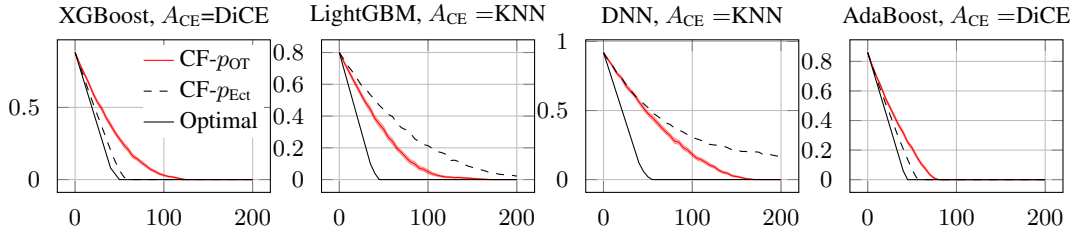


Figure 4: [German Credit] $D(f(z), y^*)$ vs. allowed actions C , with D being *MeanD*.

the divergence function D . Since CF- p_{Ect} relies on a known factual-counterfactual alignment, we benchmark the effectiveness of COLA for using this alignment. The theoretical optimality of COLA in this case can be obtained by solving an MILP, see Appendix G for how the MILP formulation is derived. Note that solving MILP is computationally heavy, hence only done for *German Credit*.

We can see that CF- p_{Ect} possess a near-optimal performance using DiCE. Remark that for DiCE and KNN, the factual-counterfactual pairs are independent to each others and hence we argue that COLA is effective for instance-based CE, even though our formulation in equation 1 is a generalization for group or distributional CE. It is interesting to note that CF- p_{OT} sometimes performs better than CF- p_{Ect} , because it utilizes a more theoretically grounded approach to identify the key features that require modification, whereas CF- p_{Ect} relies on CE algorithm-dependent knowledge, which lacks solid justification on its effectiveness for FA. We notice that there is still a gap between CF- p_{Ect} , CF- p_{OT} and the optimal result in KNN. Finding the best alignment is still an open question.

7 CONCLUSIONS

This paper introduces a novel framework, COLA, for refining CE by joint-distribution-informed Shapley values, ensuring the refined CE maintains the counterfactual effect with fewer actions.

486 ETHICS STATEMENT
487488 All authors have read and agree to abide by the ICLR Code of Ethics.⁵ This paper proposes a method
489 (*COLA* with *p-SHAP*) for refining CE. Our work is methodological and empirical; it does not involve
490 human subjects or interventions, and we did not collect, annotate, or release any new personal data.
491492 All experiments use standard, de-identified, publicly available tabular datasets (e.g., Adult/Census
493 Income, German Credit, HELOC). We follow dataset licenses/terms and the common research
494 practice of using these data solely for benchmarking. We do not attempt re-identification or linkage,
495 and we release no additional personal information. Our code will include options to exclude protected
496 attributes and to enforce feasibility/immutability constraints on features.
497498 CE can surface biases in underlying models but do not by themselves guarantee fairness. Our method
499 can reduce the number of recommended feature edits; it does *not* authorize edits to sensitive or
500 immutable attributes (e.g., sex, race, age) nor does it confer causal validity. We discourage use of
501 CE to “game” high-stakes systems (e.g., lending, hiring, healthcare) or to pressure individuals into
502 unrealistic or unethical behavior changes. Any deployment in consequential domains should include
503 domain-expert-defined feasibility constraints, fairness audits (e.g., disparate impact/benefit across
504 groups), human oversight, and compliance with applicable data-protection and AI regulations. We
505 explicitly caution that our attribution is distributional (not causal) and must not be interpreted as
506 causal effect.
507508 Risks include (i) misinterpretation of attributions as causal, (ii) recommending infeasible or harmful
509 edits, and (iii) enabling strategic manipulation. We mitigate these by (a) stating non-causal scope
510 and limitations in the paper, (b) supporting cost/feasibility masks and immutable features in the
511 implementation, (c) reporting performance across subgroups where relevant, and (d) providing
512 guidance for responsible use in documentation.
513514 We provide an anonymized implementation, detailed settings, and seeds to facilitate replication; we
515 report model types, hyperparameters, and compute budgets, and we avoid result cherry-picking by
516 using fixed evaluation protocols. To our knowledge, there are no conflicts of interest or sensitive
517 sponsorships related to this submission; any funding disclosures will be provided after the double-
518 blind review.
519520 REPRODUCIBILITY STATEMENT
521522 We take reproducibility seriously and provide pointers to all necessary components. The COLA
523 framework and p-SHAP attribution are specified with pseudocode and notation in the main paper
524 (Algorithm 1; Method and Preliminaries sections), with all theoretical assumptions and complete
525 proofs deferred to the appendix (theorems and lemmas with line-by-line proofs).
526527 Implementation details—hyperparameters, optimization settings, environment specifications, and
528 random seeds—are documented in Appendix I, which also describes the datasets used and the evalua-
529 tion protocol (including data splits and preprocessing). Baselines (models and CE generators) and
530 coupling choices are enumerated in the experimental sections and ablations, with their configurations
531 mirrored in the supplemental materials. An anonymous, downloadable code repository
532533 [Qhttps://anonymous.4open.science/r/Contrastive-Feature-Attribution-DFB1](https://anonymous.4open.science/r/Contrastive-Feature-Attribution-DFB1)
534 contains scripts to reproduce all results end-to-end, including a requirements/environment file and
535 seed-controlled runs; we also report hardware and runtime in Appendix I to contextualize compute
536 requirements, and provide ablation/sensitivity studies and the small-scale MILP benchmark setup in
537 the appendix to support independent verification.
538539 REFERENCES
540541 Google OR-Tools. URL <https://developers.google.com/optimization>.
542543 Gurobi Optimization, LLC. URL <https://www.gurobi.com>.
544550 ⁵<https://iclr.cc/public/CodeOfEthics>

540 Machine Learning in Python. URL <https://scikit-learn.org/stable/>.
 541

542 Emanuele Albini, Jason Long, Danial Dervovic, and Daniele Magazzeni. Counterfactual shapley
 543 additive explanations. In *Proceedings of the 2022 ACM Conference on Fairness, Accountability,
 544 and Transparency*, pp. 1054–1070, 2022.

545 Nuno Antonio, Ana de Almeida, and Luis Nunes. Hotel booking demand datasets. *Data in brief*, 22:
 546 41–49, 2019.
 547

548 Alejandro Barredo Arrieta, Natalia Díaz-Rodríguez, Javier Del Ser, Adrien Bennetot, Siham Tabik,
 549 Alberto Barbado, Salvador García, Sergio Gil-López, Daniel Molina, Richard Benjamins, et al.
 550 Explainable artificial intelligence (xai): Concepts, taxonomies, opportunities and challenges toward
 551 responsible ai. *Information fusion*, 58:82–115, 2020.

552 Emilio Carrizosa, Jasone Ramírez-Ayerbe, and Dolores Romero Morales. Mathematical optimization
 553 modelling for group counterfactual explanations. *European Journal of Operational Research*,
 554 2024.

555 Tianqi Chen and Carlos Guestrin. Xgboost: A scalable tree boosting system. In *Proceedings of the
 556 22nd ACM SIGKDD international conference on knowledge discovery and data mining*, pp. 785–794,
 557 2016.

558 Claudio Contardo, Ricardo Fukasawa, Louis-Martin Rousseau, and Thibaut Vidal. Optimal coun-
 559 terfactual explanations for k-nearest neighbors using mathematical optimization and constraint
 560 programming. URL <https://optimization-online.org/>.

562 Arun Das and Paul Rad. Opportunities and challenges in explainable artificial intelligence (xai): A
 563 survey. *arXiv preprint arXiv:2006.11371*, 2020.

564

565 FICO. Fico explainable machine learning challenge, 2018. URL <https://community.fico.com/s/explainable-machine-learning-challenge>.

567 Alexandre Forel, Axel Parmentier, and Thibaut Vidal. Explainable data-driven optimization: From
 568 context to decision and back again. In *International Conference on Machine Learning*, pp. 10170–
 569 10187. PMLR, 2023.

570

571 Riccardo Guidotti. Counterfactual explanations and how to find them: literature review and bench-
 572 marking. *Data Mining and Knowledge Discovery*, pp. 1–55, 2022.

573 Hans Hofmann. Statlog (German Credit Data). UCI Machine Learning Repository, 1994. DOI:
 574 <https://doi.org/10.24432/C5NC77>.

575

576 Lauren Kirchner, Jeff Larson, Surya Mattu, and J Angwin. How we analyzed the com-
 577 pas recidivism algorithm, 2016. URL [https://www.propublica.org/article/
 578 how-we-analyzed-the-compas-recidivism-algorithm](https://www.propublica.org/article/how-we-analyzed-the-compas-recidivism-algorithm).

579 Kentaro Kanamori, Takuya Takagi, Ken Kobayashi, and Hiroki Arimura. Dace: Distribution-aware
 580 counterfactual explanation by mixed-integer linear optimization. In *IJCAI*, pp. 2855–2862, 2020.

581

582 Kentaro Kanamori, Takuya Takagi, Ken Kobayashi, and Yuichi Ike. Counterfactual explanation trees:
 583 Transparent and consistent actionable recourse with decision trees. In *International Conference on
 584 Artificial Intelligence and Statistics*, pp. 1846–1870. PMLR, 2022.

585 Amir-Hossein Karimi, Bernhard Schölkopf, and Isabel Valera. Algorithmic recourse: from coun-
 586 terfactual explanations to interventions. In *Proceedings of the 2021 ACM conference on fairness,
 587 accountability, and transparency*, pp. 353–362, 2021.

588

589 Guolin Ke, Qi Meng, Thomas Finley, Taifeng Wang, Wei Chen, Weidong Ma, Qiwei Ye, and Tie-Yan
 590 Liu. Lightgbm: A highly efficient gradient boosting decision tree. *Advances in neural information
 591 processing systems*, 30, 2017.

592

593 Ramaravind Kommiya Mothilal, Divyat Mahajan, Chenhao Tan, and Amit Sharma. Towards uni-
 594 fying feature attribution and counterfactual explanations: Different means to the same end. In
 595 *Proceedings of the 2021 AAAI/ACM Conference on AI, Ethics, and Society*, pp. 652–663, 2021.

594 Yongchan Kwon and James Y Zou. Weightedshap: analyzing and improving shapley based feature
 595 attributions. *Advances in Neural Information Processing Systems*, 35:34363–34376, 2022.
 596

597 Dan Ley, Saumitra Mishra, and Daniele Magazzeni. Global counterfactual explanations: Investiga-
 598 tions, implementations and improvements. *arXiv preprint arXiv:2204.06917*, 2022.

599 Dan Ley, Saumitra Mishra, and Daniele Magazzeni. Globe-ce: a translation based approach for global
 600 counterfactual explanations. In *International Conference on Machine Learning*, pp. 19315–19342.
 601 PMLR, 2023.

602 Scott M Lundberg and Su-In Lee. A unified approach to interpreting model predictions. *Advances in
 603 neural information processing systems*, 30, 2017.

604

605 Luke Merrick and Ankur Taly. The explanation game: Explaining machine learning models using
 606 shapley values. In *Machine Learning and Knowledge Extraction: 4th IFIP TC 5, TC 12, WG
 607 8.4, WG 8.9, WG 12.9 International Cross-Domain Conference, CD-MAKE 2020, Dublin, Ireland,
 608 August 25–28, 2020, Proceedings* 4, pp. 17–38. Springer, 2020.

609

610 Ramaravind K Mothilal, Amit Sharma, and Chenhao Tan. Explaining machine learning classifiers
 611 through diverse counterfactual explanations. In *Proceedings of the 2020 conference on fairness,
 612 accountability, and transparency*, pp. 607–617, 2020.

613

614 Yasunobu Nohara, Koutarou Matsumoto, Hidehisa Soejima, and Naoki Nakashima. Explanation
 615 of machine learning models using shapley additive explanation and application for real data in
 616 hospital. *Computer Methods and Programs in Biomedicine*, 214:106584, 2022.

617

618 Axel Parmentier and Thibaut Vidal. Optimal counterfactual explanations in tree ensembles. In *International
 619 conference on machine learning*, pp. 8422–8431. PMLR, 2021.

620

621 Adam Paszke, Sam Gross, Francisco Massa, Adam Lerer, James Bradbury, Gregory Chanan, Trevor
 622 Killeen, Zeming Lin, Natalia Gimelshein, Luca Antiga, et al. Pytorch: An imperative style,
 623 high-performance deep learning library. *Advances in neural information processing systems*, 32,
 624 2019.

625

626 Kaivalya Rawal and Himabindu Lakkaraju. Beyond individualized recourse: Interpretable and
 627 interactive summaries of actionable recourses. *Advances in Neural Information Processing Systems*,
 628 33:12187–12198, 2020.

629

630 Amit Sharma, Hua Li, and Jian Jiao. The counterfactual-shapley value: Attributing change in system
 631 metrics. In *NeurIPS 2022 Workshop on Causality for Real-world Impact*.

632

633 Yi Sun and Mukund Sundararajan. Axiomatic attribution for multilinear functions. In *Proceedings of
 634 the 12th ACM conference on Electronic commerce*, pp. 177–178, 2011.

635

636 Mukund Sundararajan and Amir Najmi. The many shapley values for model explanation. In *International
 637 conference on machine learning*, pp. 9269–9278. PMLR, 2020.

638

639 Lucile Ter-Minassian, Sahra Ghalebikesabi, Karla Diaz-Ordaz, and Chris Holmes. Challenges and
 640 opportunities of shapley values in a clinical context. *arXiv preprint arXiv:2306.14698*, 2023.

641

642 Berk Ustun, Alexander Spangher, and Yang Liu. Actionable recourse in linear classification. In *Proceedings of the
 643 conference on fairness, accountability, and transparency*, pp. 10–19, 2019.

644

645 Sahil Verma, John Dickerson, and Keegan Hines. Counterfactual explanations for machine learning:
 646 A review. *arXiv preprint arXiv:2010.10596*, 2, 2020.

647

648 Sandra Wachter, Brent Mittelstadt, and Chris Russell. Counterfactual explanations without opening
 649 the black box: Automated decisions and the gdpr. *Harv. JL & Tech.*, 31:841, 2017.

650

651 Lei You, Lele Cao, Mattias Nilsson, Bo Zhao, and Lei Lei. Distributional counterfactual explanations
 652 with optimal transport. In *The 28th International Conference on Artificial Intelligence and Statistics*,
 653 2025.

654

648
649
650
APPENDICES

651	A Comparison to Existing Approaches	13
652	B \mathcal{NP}-hardness of the Problem in equation 1	13
653	C Proof of Theorem 4.1: p-SHAP Towards Counterfactual Effect	14
654	D Proof of Theorem 4.2: Interventional Effect	16
655	E Proof of Theorem 5.1: Counterfactual Proximity	17
656	F Analysis of Computational Complexity of COLA	18
657	G An MILP Formulation of equation 1 With MeanD	18
658	H Extended Numerical Results	19
659	I Experiments Reproducibility	20

664
665
666
A COMPARISON TO EXISTING APPROACHES

667 The authors in (Albini et al., 2022) proposed CF-SHAP, which uses counterfactual data points as the
 668 background distribution for Shapley. Yet, it assumes the counterfactual data distribution is defined
 669 conditionally on each single data instance, which implies that there is a known probabilistic alignment
 670 between every factual and every counterfactual instance. Similar assumptions are made in (Merrick
 671 & Taly, 2020; Kommiya Mothilal et al., 2021). In many scenarios where global explanations are
 672 expected, this assumption fails. We note that the setup in (Albini et al., 2022) for counterfactual data
 673 distribution is a special case of ours. The authors in (Kwon & Zou, 2022) proposed WeightedSHAP,
 674 adding weights to features rather than treating them as contributing equally. Our proposed method
 675 weights the contributions for data points and can be straightforwardly extended to consider weighting
 676 both rows and columns. Literature (Kommiya Mothilal et al., 2021) establishes a framework for
 677 utilizing both FA and CE for explainability. Yet, the CE-based FA have the same assumption as
 678 (Albini et al., 2022), making it difficult to generalize to group (Ley et al., 2023; 2022) or distributional
 679 CE (You et al., 2025) cases. Another relevant work is (Sharma et al.), a method that models
 680 counterfactuals using a system’s causal structure and time-series predictors to fairly decompose a
 681 single observed change in a system-level metric into contributions from individual inputs. More
 682 importantly, the aforementioned literature does not address the minimal actions CE problem, which
 683 is the focus of our paper.

684 The problems formulated in (Kanamori et al., 2022; Karimi et al., 2021) are quite close to the one
 685 investigated in this paper. In (Karimi et al., 2021) the authors minimize the cost of performing actions
 686 with assumptions of known structural causal model (SCM), which is rarely known in practice. The
 687 authors in (Kanamori et al., 2022) pointed out that it remains open whether existing CE methods can
 688 be used for solving that problem. An-MILP-solvers based approach is proposed for linear classifiers,
 689 tree ensembles, and deep ReLU networks, built upon the works (Ustun et al., 2019; Kanamori et al.,
 690 2020; Parmentier & Vidal, 2021). However, solving MILP is costly, which makes it difficult to scale.

691
692
693
B \mathcal{NP} -HARDNESS OF THE PROBLEM IN EQUATION 1

694 Theorem B.1 below states that one does not expect a scalable exact algorithm for solving it generally,
 695 unless $\mathcal{P} = \mathcal{NP}$, and the hardness lies not only on the non-linearity of f , but also its combinatorial
 696 nature.

697 **Theorem B.1.** *Problem equation 1 is generally \mathcal{NP} -hard for non-trivial divergences. More specifically, it is hard even when $d = 1$ for linear models.*

698
699
700 *Proof.* Consider the *Sparse Regression (SR) with a Cardinality Constraint* problem, defined as
 701 follows. Given a matrix $\mathbf{W} \in \mathbb{R}^{m \times n}$, a target vector $\mathbf{y}^* \in \mathbb{R}^m$, and a sparsity level $K \in \mathbb{N}$, the
 702 goal is to find a vector $\mathbf{z} \in \mathbb{R}^n$ that minimizes the residual error while having at most K non-zero

702 elements:

$$\begin{aligned} 704 \quad & \min_{\mathbf{z}} \|\mathbf{Wz} - \mathbf{y}^*\|_2^2 \\ 705 \quad & \text{s.t. } \|\mathbf{z}\|_0 \leq K, \end{aligned}$$

706 where $\|\mathbf{z}\|_0$ denotes the number of non-zero elements in \mathbf{z} . This problem is known to be \mathcal{NP} -hard
707 due to the combinatorial nature of selecting the subset of variables to include in the model.
708

709 We will map this SR problem to our problem equation 1 with the following settings. Let the number
710 of features be $d = 1$ and the number of instances be n (the same as the dimension of the SR problem).
711 Let the factual data be $\mathbf{x} = \mathbf{0} \in \mathbb{R}^n$ (the zero vector), and the target model output be $\mathbf{y}^* \in \mathbb{R}^m$ (as
712 given in the SR problem). We define the model f as a linear function $f(\mathbf{z}) = \mathbf{Wz}$.

713 For the model output, we define $D(f(\mathbf{z}), \mathbf{y}^*) = \|f(\mathbf{z}) - \mathbf{y}^*\|_2^2$, i.e. the Euclidean distance squared.
714 For the instances, we define $D(\mathbf{z}, \mathbf{x}) = \|\mathbf{z} - \mathbf{x}\|_2^2 = \|\mathbf{z}\|_2^2$, since $\mathbf{x} = \mathbf{0}$. We set the maximum allowed
715 feature changes C to be equal to k (the sparsity level from the SR problem). The large constant M
716 can be any sufficiently large positive number, for example, $M \geq \max_i |z_i|$.

717 Given that $\mathbf{x} = \mathbf{0}$, constraints equation 1d and equation 1e simplify to:

$$\begin{aligned} 719 \quad z_i & \leq 0 \cdot (1 - c_i) + Mc_i = Mc_i, \\ 720 \quad z_i & \geq 0 \cdot (1 - c_i) - Mc_i = -Mc_i, \quad \forall k = 1, \dots, n. \end{aligned}$$

721 This means that if $c_i = 0$, then $z_i \leq 0$ and $z_i \geq 0$, so $z_i = 0$. If $c_i = 1$, then $z_i \in [-M, M]$. The
722 constraint equation 1c becomes $\sum_{k=1}^n c_i \leq k$.

723 Our problem equation 1 thus becomes:

$$\min_{\mathbf{c}, \mathbf{z}} \|\mathbf{Wz} - \mathbf{y}^*\|_2^2 \tag{11a}$$

$$\text{s.t. } \|\mathbf{z}\|_2^2 \leq \epsilon \tag{11b}$$

$$\sum_{k=1}^d c_i \leq k \tag{11c}$$

$$z_i = 0, \quad \text{if } c_i = 0 \tag{11d}$$

$$z_i \in [-M, M], \quad \text{if } c_i = 1 \tag{11e}$$

$$c_i \in \{0, 1\}, \quad \forall k = 1, \dots, n. \tag{11f}$$

735 In this formulation, the variables c_i indicate whether the variable z_i is allowed to change ($c_i = 1$) or
736 not ($c_i = 0$). The constraints enforce that $z_i = 0$ when $c_i = 0$, mirroring the sparsity constraint in
737 the SR problem. The constraint $\sum_{k=1}^n c_i \leq k$ ensures that at most k features can change, matching
738 the sparsity level. The objective function is identical to that of SR.

740 Since our problem formulation directly mirrors the SR problem with a cardinality constraint, which
741 is known to be \mathcal{NP} -hard, solving Problem equation 1 is at least as hard as solving the SR problem.
742 Therefore, Problem equation 1 is \mathcal{NP} -hard even when $d = 1$, the model f is linear, and the divergence
743 functions D are standard Euclidean distances. \square

745 C PROOF OF THEOREM 4.1: p -SHAP TOWARDS COUNTERFACTUAL EFFECT

747 Let $\mathbf{x} = \{\mathbf{x}_i\}_{i=1}^n \in \mathbb{R}^{n \times d}$ be the set of factual data points with associated probability weights $\mu_i \geq 0$
748 such that $\sum_{i=1}^n \mu_i = 1$, and let $\mathbf{r} = \{\mathbf{r}_j\}_{j=1}^m \in \mathbb{R}^{m \times d}$ be the set of counterfactual data points with
749 associated probability weights $\nu_j \geq 0$ such that $\sum_{j=1}^m \nu_j = 1$. Let $\mathbf{p}_{\text{OT}} \in \mathbb{R}^{n \times m}$ be the OT plan
750 between \mathbf{x} and \mathbf{r} that minimizes the expected transportation cost:

$$752 \quad \mathbf{p}_{\text{OT}} = \arg \min_{\mathbf{p} \in \Pi(\boldsymbol{\mu}, \boldsymbol{\nu})} \sum_{i=1}^n \sum_{j=1}^m p_{ij} \|\mathbf{x}_i - \mathbf{r}_j\|_2^2,$$

753 where $\Pi(\boldsymbol{\mu}, \boldsymbol{\nu})$ is the set of joint distributions satisfying the marginal constraints $\sum_{j=1}^m p_{ij} = \mu_i$ for
754 all i and $\sum_{i=1}^n p_{ij} = \nu_j$ for all j . The theorem below provides that feature attributions are aligned

756 with the expected costs of feature modifications, leading to action plans that are cost-efficient in
 757 achieving counterfactual outcomes.

758 **Theorem C.1** (Theorem 4.1 in the main text). *Consider the 1-Wasserstein divergence W_1 , i.e.
 759 $W_1(f(\mathbf{x}), \mathbf{y}^*) = \min_{\pi \in \Pi} \sum_{i=1}^n \sum_{j=1}^m \pi_{ij} |f(\mathbf{x}_i) - \mathbf{y}_j^*|$. Suppose the counterfactual outcome \mathbf{y}^* is
 760 fully achieved by \mathbf{r} , i.e. $\mathbf{y}_j^* = f(\mathbf{r}_j)$ ($j = 1, 2, \dots, m$). Assume that the model $f : \mathbb{R}^d \rightarrow \mathbb{R}$ is Lipschitz
 761 continuous with Lipschitz constant L . The expected absolute difference in model outputs between the
 762 factual and counterfactual instances, weighted by \mathbf{p}_{OT} (with $\varepsilon = 0$), is bounded by:
 763*

$$764 \quad W_1(f(\mathbf{x}), \mathbf{y}^*) \leq L \sqrt{\sum_{i=1}^n \sum_{j=1}^m p_{ij}^{\text{OT}} \|\mathbf{x}_i - \mathbf{r}_j\|_2^2} \leq L \sqrt{\sum_{i=1}^n \sum_{j=1}^m p_{ij} \|\mathbf{x}_i - \mathbf{r}_j\|_2^2} \quad \forall \mathbf{p} \in \Pi.$$

767 *Namely, \mathbf{p}_{OT} minimizes the upper bound of $W_1(f(\mathbf{x}), \mathbf{y}^*)$, where the upper bound is based on the
 768 expected feature modification cost.*

770 *Proof.* Since the model f is Lipschitz continuous with constant L , for any $\mathbf{x}_i \in \mathbb{R}^d$ and $\mathbf{r}_j \in \mathbb{R}^d$, it
 771 holds that:

$$772 \quad |f(\mathbf{x}_i) - f(\mathbf{r}_j)| \leq L \|\mathbf{x}_i - \mathbf{r}_j\|_2.$$

773 Multiplying both sides of the inequality by $p_{ij}^{\text{OT}} \geq 0$, we obtain:

$$775 \quad p_{ij}^{\text{OT}} |f(\mathbf{x}_i) - f(\mathbf{r}_j)| \leq L p_{ij}^{\text{OT}} \|\mathbf{x}_i - \mathbf{r}_j\|_2.$$

776 Summing both sides over all $i = 1, \dots, n$ and $j = 1, \dots, m$, we have:

$$778 \quad \sum_{i=1}^n \sum_{j=1}^m p_{ij}^{\text{OT}} |f(\mathbf{x}_i) - f(\mathbf{r}_j)| \leq L \sum_{i=1}^n \sum_{j=1}^m p_{ij}^{\text{OT}} \|\mathbf{x}_i - \mathbf{r}_j\|_2.$$

781 Let us denote $E_f = \sum_{i=1}^n \sum_{j=1}^m p_{ij}^{\text{OT}} |f(\mathbf{x}_i) - f(\mathbf{r}_j)|$ and $E_d = \sum_{i=1}^n \sum_{j=1}^m p_{ij}^{\text{OT}} \|\mathbf{x}_i - \mathbf{r}_j\|_2$. The
 782 inequality then becomes:

$$783 \quad E_f \leq L E_d.$$

784 To further bound E_d , we apply the Cauchy-Schwarz inequality. Observe that the weights p_{ij}^{OT} are
 785 non-negative and satisfy $\sum_{i=1}^n \sum_{j=1}^m p_{ij}^{\text{OT}} = 1$ because \mathbf{p}_{OT} is a probability distribution over the joint
 786 space of \mathbf{x} and \mathbf{r} . The Cauchy-Schwarz inequality states that for any real-valued functions a_{ij} and
 787 b_{ij} ,

$$789 \quad \left(\sum_{i,j} a_{ij} b_{ij} \right)^2 \leq \left(\sum_{i,j} a_{ij}^2 \right) \left(\sum_{i,j} b_{ij}^2 \right).$$

792 Setting $a_{ij} = \sqrt{p_{ij}^{\text{OT}}}$ and $b_{ij} = \sqrt{p_{ij}^{\text{OT}}} \|\mathbf{x}_i - \mathbf{r}_j\|_2$, we have:

$$794 \quad E_d = \sum_{i,j} p_{ij}^{\text{OT}} \|\mathbf{x}_i - \mathbf{r}_j\|_2 = \sum_{i,j} \sqrt{p_{ij}^{\text{OT}}} \sqrt{p_{ij}^{\text{OT}}} \|\mathbf{x}_i - \mathbf{r}_j\|_2 = \sum_{i,j} a_{ij} b_{ij}.$$

796 Applying the Cauchy-Schwarz inequality:

$$798 \quad E_d^2 \leq \left(\sum_{i,j} a_{ij}^2 \right) \left(\sum_{i,j} b_{ij}^2 \right) = \left(\sum_{i,j} p_{ij}^{\text{OT}} \right) \left(\sum_{i,j} p_{ij}^{\text{OT}} \|\mathbf{x}_i - \mathbf{r}_j\|_2^2 \right).$$

802 Since $\sum_{i,j} p_{ij}^{\text{OT}} = 1$, this simplifies to:

$$803 \quad E_d^2 \leq \sum_{i=1}^n \sum_{j=1}^m p_{ij}^{\text{OT}} \|\mathbf{x}_i - \mathbf{r}_j\|_2^2 = \sum_{i=1}^n \sum_{j=1}^m p_{ij}^{\text{OT}} \|\mathbf{x}_i - \mathbf{r}_j\|_2^2.$$

806 Taking the square root of both sides, we obtain:

$$808 \quad E_d \leq \sqrt{\sum_{i=1}^n \sum_{j=1}^m p_{ij}^{\text{OT}} \|\mathbf{x}_i - \mathbf{r}_j\|_2^2}.$$

810 Substituting back into the inequality for E_f , we have:
 811

$$812 \quad 813 \quad 814 \quad 815 \quad E_f \leq L \sqrt{\sum_{i=1}^n \sum_{j=1}^m p_{ij}^{\text{OT}} \|\mathbf{x}_i - \mathbf{r}_j\|_2^2}.$$

816 Note that the 1-Wasserstein divergence is no more than E_f ⁶, then,
 817

$$818 \quad 819 \quad 820 \quad W_1(f(\mathbf{x}), \mathbf{y}^*) = \min_{\pi \in \Pi} \sum_{i=1}^n \sum_{j=1}^m \pi_{ij} |f(\mathbf{x}_i) - \mathbf{y}_j^*| \leq E_f \leq L \sqrt{\sum_{i=1}^n \sum_{j=1}^m p_{ij}^{\text{OT}} \|\mathbf{x}_i - \mathbf{r}_j\|_2^2}.$$

821 Therefore, the 1-Wasserstein divergence between $f(\mathbf{x})$ and \mathbf{y}^* is bounded by the Lipschitz constant
 822 L times the square root of the expected transportation cost under \mathbf{p}_{OT} . Since \mathbf{p}_{OT} minimizes the
 823 expected transportation cost $\sum_{i,j} p_{ij} \|\mathbf{x}_i - \mathbf{r}_j\|_2^2$ over all feasible transport plans in $\Pi(\boldsymbol{\mu}, \boldsymbol{\nu})$, we have
 824

$$825 \quad 826 \quad 827 \quad 828 \quad \sqrt{\sum_{i=1}^n \sum_{j=1}^m p_{ij}^{\text{OT}} \|\mathbf{x}_i - \mathbf{r}_j\|_2^2} \leq \sqrt{\sum_{i=1}^n \sum_{j=1}^m p_{ij} \|\mathbf{x}_i - \mathbf{r}_j\|_2^2} \quad \forall \mathbf{p} \in \Pi(\boldsymbol{\mu}, \boldsymbol{\nu}).$$

829 Hence the conclusion. □
 830

831 D PROOF OF THEOREM 4.2: INTERVENTIONAL EFFECT

832
 833 **Theorem D.1** (Theorem 4.2 in the main text). *For any subset $S \subseteq \mathcal{F}$ and any \mathbf{x}_i ($i = 1, 2, \dots, n$),
 834 $v^{(i)}(S)$ represents the causal effect of the difference between the expected value of $f(\mathbf{r})$ under the
 835 intervention on features S and the unconditional expected value of $f(\mathbf{r})$. Mathematically, this is
 836 expressed as:*

$$837 \quad 838 \quad \mathbb{E}[f(\mathbf{r})] + v^{(i)}(S) = \mathbb{E}[f(\mathbf{r}) | \text{do}(\mathbf{r}_S = \mathbf{x}_{i,S})].$$

839
 840 *Proof.* Let $p(\mathbf{x}, \mathbf{r})$ be the joint probability of \mathbf{x} and \mathbf{r} obtained from A_{Prob} . Under the intervention
 841 $\text{do}(\mathbf{r}_S = \mathbf{x}_{i,S})$, the features in S are set to $\mathbf{x}_{i,S}$, and the features in $\mathcal{F} \setminus S$ remain distributed according
 842 to their marginal distribution $p(\mathbf{r}_{\mathcal{F} \setminus S})$. Therefore, the expected value of $f(\mathbf{r})$ under the intervention
 843 is:

$$844 \quad 845 \quad \mathbb{E}[f(\mathbf{r}) | \text{do}(\mathbf{r}_S = \mathbf{x}_{i,S})] = \int_{\mathcal{R}_{\mathcal{F} \setminus S}} f(\mathbf{x}_{i,S}; \mathbf{r}_{\mathcal{F} \setminus S}) p(\mathbf{r}_{\mathcal{F} \setminus S}) d\mathbf{r}_{\mathcal{F} \setminus S}.$$

846 Remark that by the definition of $v^{(i)}(S)$,
 847

$$848 \quad 849 \quad 850 \quad v^{(i)}(S) = \mathbb{E}_{\mathbf{r} \sim p(\mathbf{r} | \mathbf{x}_i)} [f(\mathbf{x}_{i,S}; \mathbf{r}_{\mathcal{F} \setminus S})] - \mathbb{E}[f(\mathbf{r})] = \int_{\mathcal{R}_{\mathcal{F} \setminus S}} f(\mathbf{x}_{i,S}; \mathbf{r}_{\mathcal{F} \setminus S}) p(\mathbf{r}_{\mathcal{F} \setminus S}) d\mathbf{r}_{\mathcal{F} \setminus S} - \mathbb{E}[f(\mathbf{r})],$$

851 such that

$$852 \quad 853 \quad \mathbb{E}[f(\mathbf{r})] + v^{(i)}(S) = \mathbb{E}[f(\mathbf{r}) | \text{do}(\mathbf{r}_S = \mathbf{x}_{i,S})].$$

854 Hence the conclusion. □
 855

856 The value function $v^{(i)}(S)$ captures the expected value of $f(\mathbf{r})$ when we intervene by setting the
 857 features in S to $\mathbf{x}_{i,S}$, denoted as $\text{do}(\mathbf{r}_S = \mathbf{x}_{i,S})$. This intervention is independent of any predefined
 858 joint probability distribution $p(\mathbf{x}, \mathbf{r})$. Therefore, the expression $\mathbb{E}[f(\mathbf{r})] + v^{(i)}(S)$ represents the
 859 combined effect of the base expected value of $f(\mathbf{r})$ and the additional causal impact of the attribution
 860 $v^{(i)}(S)$.
 861

862 ⁶Note that $E_f = \sum_{i=1}^n \sum_{j=1}^m p_{ij}^{\text{OT}} |f(\mathbf{x}_i) - f(\mathbf{r}_j)|$. Because both π and \mathbf{p}_{OT} denote joint probability of \mathbf{x}
 863 and \mathbf{r} , however, π makes the summation the minimum for the W_1 term across all possible joint distributions,
 whereas \mathbf{p}_{OT} does not.

864 E PROOF OF THEOREM 5.1: COUNTERFACTUAL PROXIMITY
865

866 **Theorem E.1** (Theorem 5.1 in the main text). *Let $\mathbf{q} \in \mathbb{R}^{n \times d}$ be the aligned reference matrix derived
867 from the counterfactual set $\mathbf{r} \in \mathbb{R}^{m \times d}$ via the value assignment step $\mathbf{q} = A_{\text{Value}}(\mathbf{r}, \mathbf{p})$, where \mathbf{p} is
868 the coupling matrix. For any dimensions $n, m \geq 1$, the refined counterfactual \mathbf{z} constructed by the
869 COLA framework satisfies:*

$$870 \quad \|\mathbf{z} - \mathbf{x}\|_F \leq \|\mathbf{q} - \mathbf{x}\|_F.$$

871 *This inequality guarantees that the refined counterfactual \mathbf{z} is strictly closer (or equal) to the factual
872 input \mathbf{x} compared to the aligned counterfactual proposal \mathbf{q} , ensuring that the refinement process
873 introduces no additional divergence.*

874 *Proof.* Let \mathbf{q} be the aligned reference matrix generated by $A_{\text{Value}}(\mathbf{r}, \mathbf{p})$. For the elements where
875 $c_{ik} = 1$ (modified elements), $z_{ik} = q_{ik}$. For elements where $c_{ik} = 0$, $z_{ik} = x_{ik}$. Therefore, we can
876 write:

$$877 \quad (z_{ik} - x_{ik})^2 = \begin{cases} (q_{ik} - x_{ik})^2, & \text{if } c_{ik} = 1, \\ 0, & \text{if } c_{ik} = 0. \end{cases} \quad (12)$$

878 The squared Frobenius norms with respect to \mathbf{q} and \mathbf{z} are computed as follows:

$$879 \quad \|\mathbf{q} - \mathbf{x}\|_F^2 = \sum_{i=1}^n \sum_{k=1}^d (q_{ik} - x_{ik})^2,$$

$$880 \quad \|\mathbf{z} - \mathbf{x}\|_F^2 = \sum_{i=1}^n \sum_{k=1}^d (z_{ik} - x_{ik})^2.$$

881 And,

$$882 \quad \|\mathbf{q} - \mathbf{x}\|_F^2 - \|\mathbf{z} - \mathbf{x}\|_F^2 = \sum_{i=1}^n \sum_{k=1}^d (q_{ik} - x_{ik})^2 - \sum_{i=1}^n \sum_{k=1}^d (z_{ik} - x_{ik})^2$$

$$883 \stackrel{(i)}{=} \sum_{i=1}^n \sum_{k=1}^d (q_{ik} - x_{ik})^2 - \sum_{(i,k):c_{ik}=1} (q_{ik} - x_{ik})^2$$

$$884 = \sum_{(i,k):c_{ik}=0} (q_{ik} - x_{ik})^2 \geq 0,$$

885 where the equality (i) holds because of equation 12.

886 Since the difference $\|\mathbf{q} - \mathbf{x}\|_F^2 - \|\mathbf{z} - \mathbf{x}\|_F^2 \geq 0$, it follows that:

$$887 \quad \|\mathbf{z} - \mathbf{x}\|_F^2 \leq \|\mathbf{q} - \mathbf{x}\|_F^2.$$

888 Taking square roots, we get:

$$889 \quad \|\mathbf{z} - \mathbf{x}\|_F \leq \|\mathbf{q} - \mathbf{x}\|_F.$$

890 Hence the conclusion. □

891 **Corollary E.2** (Corollary 5.2 in the main text). *In the special case where $n = m$ and the OT plan \mathbf{p}
892 corresponds to a deterministic permutation σ (i.e., obtained without entropic regularization, $\varepsilon = 0$),
893 the matrix \mathbf{q} becomes a row-permuted version of \mathbf{r} (denoted as \mathbf{r}_σ , where $q_i = r_{\sigma(i)}$). In this setting,
894 the bound simplifies to:*

$$895 \quad \|\mathbf{z} - \mathbf{x}\|_F \leq \|\mathbf{r}_\sigma - \mathbf{x}\|_F,$$

896 *recovering the intuition that the refined counterfactual is at least as close to the factuals as the
897 original counterfactual set reordered by σ .*

898 *Proof.* Under the assumptions $n = m$ and $\varepsilon = 0$, the optimal transport plan \mathbf{p} becomes a permutation
899 matrix associated with a bijection σ . Consequently, the value assignment algorithm A_{Value} (whether
900 maximizing or averaging) assigns $q_i = r_{\sigma(i)}$ for every instance i . Substituting \mathbf{q} with the permuted
901 matrix \mathbf{r}_σ into the general bound established in Theorem 5.1 (i.e., $\|\mathbf{z} - \mathbf{x}\|_F \leq \|\mathbf{q} - \mathbf{x}\|_F$) directly
902 yields the result. □

918 **F ANALYSIS OF COMPUTATIONAL COMPLEXITY OF COLA**
 919

920 We perform analysis of the computational complexity of COLA as follows.
 921

922 First, we analyze A_{Prob} . If the alignment between \mathbf{x} and \mathbf{r} is known a priori, then A_{Prob} just constructs
 923 the matrix \mathbf{p} with the prior knowledge, which takes $O(n \times m)$. Otherwise, we consider solving OT
 924 to obtain \mathbf{p} , which, by the Sinkhorn–Knopp algorithm, takes $O(n \times m \times \log(1/\varepsilon))$.

925 Then we analyze A_{Shap} . For each subset, the model is evaluated on all n data points, leading to $O(n)$
 926 evaluations per subset. Incorporating baseline values from the reference data \mathbf{r} involves replacing
 927 the values of certain features with their corresponding baseline values. This operation is $O(m)$
 928 because it requires accessing the baseline values from the reference table \mathbf{r} for each of the d features.
 929 If we assume that the reference values can be precomputed and accessed in constant time, then
 930 the complexity of incorporating these values can be considered as $O(d)$. The number of M_{Shap}
 931 subsets results in M_{Shap} model evaluations. Combining the above steps, the complexity of A_{Shap} is
 932 $O(n \times d \times M_{\text{Shap}})$.
 933

The normalization in line 4 of COLA takes $O(n \times d)$.

934 To compare the complexities of the two algorithms, A_{Value}^{\max} and $A_{\text{Value}}^{\text{avg}}$, we analyze each algorithm
 935 step-by-step. For A_{Value}^{\max} , for each row \mathbf{x}_i in the data table, we need to (1) compute the probabilities
 936 p_{ij} for all $j \in \{1, 2, \dots, m\}$, which involves $O(m)$ operations per row, (2) identify the row \mathbf{r}_j
 937 in the reference data with the highest probability p_{ij} , which involves $O(m)$ operations per row,
 938 and (3) assign $q_{ik} = r_{\tau(i),k}$ where $\tau(i) = \arg \max_j p_{ij}$, which involves $O(d)$ operations per row.
 939 Since there are n rows in the data table, the total complexity for A_{Value}^{\max} is $O(n \times (m + m + d)) =$
 940 $O(n \times (2m + d)) = O(n \times m + n \times d) = O(n \times (m + d))$.

941 For $A_{\text{Value}}^{\text{avg}}$, for each row \mathbf{x}_i in the data table, we need to 1) compute the probabilities p_{ij} for all $j \in$
 942 $\{1, 2, \dots, m\}$, which involves $O(m)$ operations per row, 2) compute the sum $\sum_{j'=1}^m p_{ij'}$, which in-
 943 volves $O(m)$ operations per row, and 3) calculate the weighted average $q_{ik} = \sum_{j=1}^m \left(\frac{p_{ij}}{\sum_{j'=1}^m p_{ij'}} \right) r_{jk}$,
 944 which involves $O(m \times d)$ operations per row. Since there are n rows in the data table, the total
 945 complexity for $A_{\text{Value}}^{\text{avg}}$ is $O(n \times (m + m + m \times d)) = O(n \times (2m + m \times d)) = O(n \times (m + m \times d)) =$
 946 $O(n \times m \times (1 + d)) = O(n \times m \times d)$.

947 For lines 6–16, the entire complexity is straightforwardly $O(n \times d) + O(C) = O(n \times d)$ due to the
 948 fact $C \leq n \times d$.

949 Therefore, the complexity of COLA using A_{Value}^{\max} equals
 950

$$952 \quad O(M_{\text{CE}}) + O(nm \log(1/\varepsilon)) + O(ndM_{\text{Shap}}) + O(nd) + O(n(m + d)) + O(nd) \\ 953 \quad = O(M_{\text{CE}}) + O(nm \log(1/\varepsilon)) + O(ndM_{\text{Shap}}) + O(nm) + O(nd) \\ 954$$

955 and the complexity of COLA using $A_{\text{Value}}^{\text{avg}}$ equals
 956

$$957 \quad O(M_{\text{CE}}) + O(nm \log(1/\varepsilon)) + O(ndM_{\text{Shap}}) + O(nd) + O(nmd) + O(nd) \\ 958 \quad = O(M_{\text{CE}}) + O(nm \log(1/\varepsilon)) + O(ndM_{\text{Shap}}) + O(nmd)$$

959 Hence the complexity of COLA with respect to n, m, d , and the regularization parameter ε of entropic
 960 OT is
 961

$$962 \quad O(M_{\text{CE}}) + O(nm \log(1/\varepsilon)) + O(ndM_{\text{Shap}}) + N$$

963 where $N = O(nm) + O(nd)$ if A_{Value}^{\max} is used and $N = O(nmd)$ if $A_{\text{Value}}^{\text{avg}}$ is used.
 964

965 **G AN MILP FORMULATION OF EQUATION 1 WITH MEAND**
 966

967 In this section, we provide a global optimality benchmark for using a known alignment between
 968 factual and counterfactual in solving equation 1 with D being MeanD, namely
 969

$$970 \quad D(f(\mathbf{z}), \mathbf{y}^*) = \left| \frac{1}{n} \sum_{i=1}^n f(\mathbf{z}_i) - \bar{y}^* \right| \\ 971$$

972 with $\bar{y}^* = \frac{1}{m} \sum_{j=1}^m y_j^*$. Since COLA is used, we have $D(\mathbf{r}, \mathbf{x}) \leq \epsilon$, and \mathbf{z} stays closer to \mathbf{x} than \mathbf{r} ,
 973 hence equation 1b is dropped. The formulation of equation 1 then becomes:
 974

$$975 \quad \min_{\mathbf{c}, \mathbf{z}} \quad \left| \sum_{i=1}^n f(\mathbf{z}_i) - ny^* \right| \quad (13a)$$

$$978 \quad \text{s.t.} \quad \sum_{i=1}^n \sum_{k=1}^d c_{ik} \leq C \quad (13b)$$

$$980 \quad z_{ik} = r_{ik}c_{ik} + x_{ik}(1 - c_{ik}) \quad i = 1, \dots, n, \quad k = 1, \dots, d \quad (13c)$$

982 Note that the original constraints equation 1d and equation 1e merge to be equation 13c, because
 983 $CF-p_{\text{Ect}}$ is imposed to be used. That is, for any \mathbf{x}_i , there is an exact \mathbf{r}_j serves as its reference in A_{Shap}
 984 and A_{Value} , such that x_{ik} ($k = 1, 2, \dots, d$) either stays unchanged or can be changed to r_{jk} . Therefore
 985 $z_{ik} = r_{ik}c_{ik} + x_{ik}(1 - c_{ik})$ of which the value depends on the binary variable c_{ik} .

986 Due to the known alignment between any \mathbf{x}_i and its corresponding \mathbf{r}_j , \mathbf{q} is determined (also, both
 987 A_{Values}^{\max} and $A_{\text{Values}}^{\text{avg}}$ return the same \mathbf{q}). For any data point i and any feature set $S \subseteq \mathcal{F}$, let \mathbf{z}_{iS} denotes
 988 the solution \mathbf{z}_i where we have all features $k \in S$ changed to q_{ik} , and the other features $h \in \mathcal{F} \setminus S$
 989 stays x_{ih} . Hence the set of \mathbf{z}_{iS} ($S \subseteq \mathcal{F}$) composes the domain of all possible values of \mathbf{z} . Define a
 990 corresponding scalar variable for any \mathbf{z}_{iS} :

$$991 \quad g_{iS} = f(\mathbf{z}_{iS}) - \bar{y}^*.$$

993 Then, for any \mathbf{z}_i in equation 13, the value of the term $\sum_{i=1}^n f(z_i) - ny^*$ can be represented by a
 994 binary variable a_{iS} together with the scalar g_{iS} , namely,

$$995 \quad \sum_{i=1}^n f(\mathbf{z}_i) - ny^* = \sum_{i=1}^n \sum_{S \subseteq \mathcal{F}} g_{iS} a_{iS}.$$

998 The optimization problem equation 13 is hence reformulated as a mixed integer programming below.
 999

$$1000 \quad \min_{\mathbf{a}, \eta} \quad \eta \quad (14a)$$

$$1001 \quad \text{s.t.} \quad \sum_{i=1}^n \sum_{S \subseteq \mathcal{F}} g_{iS} a_{iS} \leq \eta \quad (14b)$$

$$1004 \quad \sum_{i=1}^n \sum_{S \subseteq \mathcal{F}} g_{iS} a_{iS} \geq -\eta \quad (14c)$$

$$1008 \quad \sum_{S \subseteq \mathcal{F}} a_{iS} = 1 \quad i = 1, \dots, n \quad (14d)$$

$$1010 \quad \sum_{i=1}^n \sum_{S \subseteq \mathcal{F}} |S| a_{iS} \leq C \quad (14e)$$

1012 Minimizing η under the two constraints equation 14b and equation 14c is equivalent to minimizing
 1013 the objective function of equation 13. The constraints in equation 14d guarantees that each data point
 1014 i is subject to one and only one feature modification plan a_{iS} for a specific S ($S \subseteq \mathcal{F}$). The constraint
 1015 equation 14e corresponds to equation 13b. Solving equation 14 yields the theoretical optimality of
 1016 COLA using a known alignment between factual and counterfactual, demonstrated in Figure 4 in
 1017 Section 6.

1019 H EXTENDED NUMERICAL RESULTS

1021 Observing Figures 5–8, $CF-p_{\text{Uni}}$ generally performs better than $RB-p_{\text{Uni}}$. Second, consider $RB-p_{\text{OT}}$
 1022 and $CF-p_{\text{OT}}$ that also differ only in A_{Shap} , the latter consistently outperforms the former. Hence
 1023 $RB\text{-SHAP}$ is not suitable for FA in CE.

1024 We analyze how different Shapley methods affect FA, corresponding to lines 3–4 in COLA. The
 1025 shapley methods can be classified into two categories: First, consider $RB-p_{\text{Uni}}$ and $CF-p_{\text{Uni}}$ that differ

1026 only in A_{Shap} . Observing Figures 5–8, CF- p_{Uni} generally performs better than RB- p_{Uni} . Second,
 1027 consider RB- p_{OT} and CF- p_{OT} that also differ only in A_{Shap} , the latter consistently outperforms the
 1028 former. Hence *RB-SHAP is not suitable for FA in CE*.

1029 Besides FA, the other equally important step of COLA is line 5, i.e. using the joint probability $p(\mathbf{x}, \mathbf{r})$
 1030 to compose the matrix \mathbf{q} , telling the factual x to which direction to change its features so as to move
 1031 towards the target model outcome. We observe in Figures 5–8 that CF- p_{OT} consistently outperforms
 1032 all other methods throughout all experiments. Note that all the three methods CF- p_{Uni} , CF- p_{Rnd} , and
 1033 CF- p_{OT} provide solution’s for the joint probability \mathbf{p} when the exact alignment between factuals and
 1034 counterfactuals are unknown. Yet, their performance differ significantly. Simply knowing the CE
 1035 (and its marginal distribution) is insufficient.

1036 OT proves to be exceptionally useful when the alignment information between factual and counterfac-
 1037 tual instances is missing or inaccurate. Even when the CE algorithm explicitly matches each factual
 1038 instance to a corresponding counterfactual, it is challenging to justify that the known alignment
 1039 optimizes performance. This is supported by Figure 4 in Section 6.

1040 Note that p_{OT} does not need to be the true joint distribution of \mathbf{x} and \mathbf{r} from a data generation
 1041 perspective. Instead, it should guide COLA to treat \mathbf{x} and \mathbf{r} together for both FA and CE. Furthermore,
 1042 the QDA column in Figure 5 shows stableness of OT-based methods, while others diverge significantly
 1043 from the target. We emphasize that COLA, however, is *not limited to using OT as A_{Prob}* . As indicated
 1044 by Figure 4, any known best \mathbf{p} still has non-negligible gap to the global optimality. Devising a better
 1045 A_{Prob} algorithm is hence an interesting topic worth exploration.

1047 I EXPERIMENTS REPRODUCIBILITY

1049 The experiments are conducted on a high performance computing (HPC) cluster, running with four
 1050 nodes (for the four datasets) in parallel, with each node equipped with two Intel Xeon Processor
 1051 2660v3 (10 core, 2.60GHz) and 128 GB memory. The experiment runs approximately 5-10 hours in
 1052 each node, dependent on the size of the dataset. It is also possible to reproduce the experiment on a
 1053 laptop, while it costs more computational time generally than using an HPC cluster.

1054 For the four datasets, the numerical features are standardized, and the categorical features follow
 1055 either label-encoding or one-hot encoding. Practically, we did not observe remarkable difference
 1056 between the two encoding methods in terms of COLA’s performance. The train-test split follows
 1057 7 : 3.

1058 The optimality baseline as shown in Figure 4 is solved by Gurobi 11.0.2 (gur). In order to reproduce
 1059 the optimality baseline, a license of Gurobi is required. Otherwise, we can resort to open-source
 1060 operations research libraries such as Google-OR tools (goo). We remark that solving the MILP in
 1061 Appendix G is computationally expensive, such that it may only apply to small scale datasets such as
 1062 German Credit. If one wants to compute the optimality baseline for other datasets, then the number
 1063 of used features needs to be reduced.

1064 The hyperparameters of the models used in the experiment are specified as follows. The models
 1065 Bagging, GP, RBF, RndForest, AdaBoost, GradBoost, and QDA are scikit-learn models (skl), where
 1066 all hyper-parameters are kept default. The models DNN, SVM, RBF, and LR are implemented
 1067 by PyTorch (Paszke et al., 2019). The DNN has three layers. The SVM uses the linear kernel.
 1068 The models XGBoost (Chen & Guestrin, 2016) and LightGBM (Ke et al., 2017) are used by their
 1069 scikit-learn interface, with all hyper-parameters kept default.

1071 THE USE OF LARGE LANGUAGE MODELS (LLMs)

1073 We used large language models (LLMs) only as general-purpose assist tools. Their role was limited
 1074 to grammar, wording, and light copy-editing of author-written text. LLMs did not contribute research
 1075 ideation, modeling choices, experimental design, or results. All algorithms, proofs, datasets, and
 1076 analyses were created and verified by the authors. Any LLM-suggested phrasing was reviewed and
 1077 edited before inclusion in the paper. The authors take full responsibility for all content; LLMs are not
 1078 authors or contributors. This disclosure complies with the ICLR policy on LLM usage.

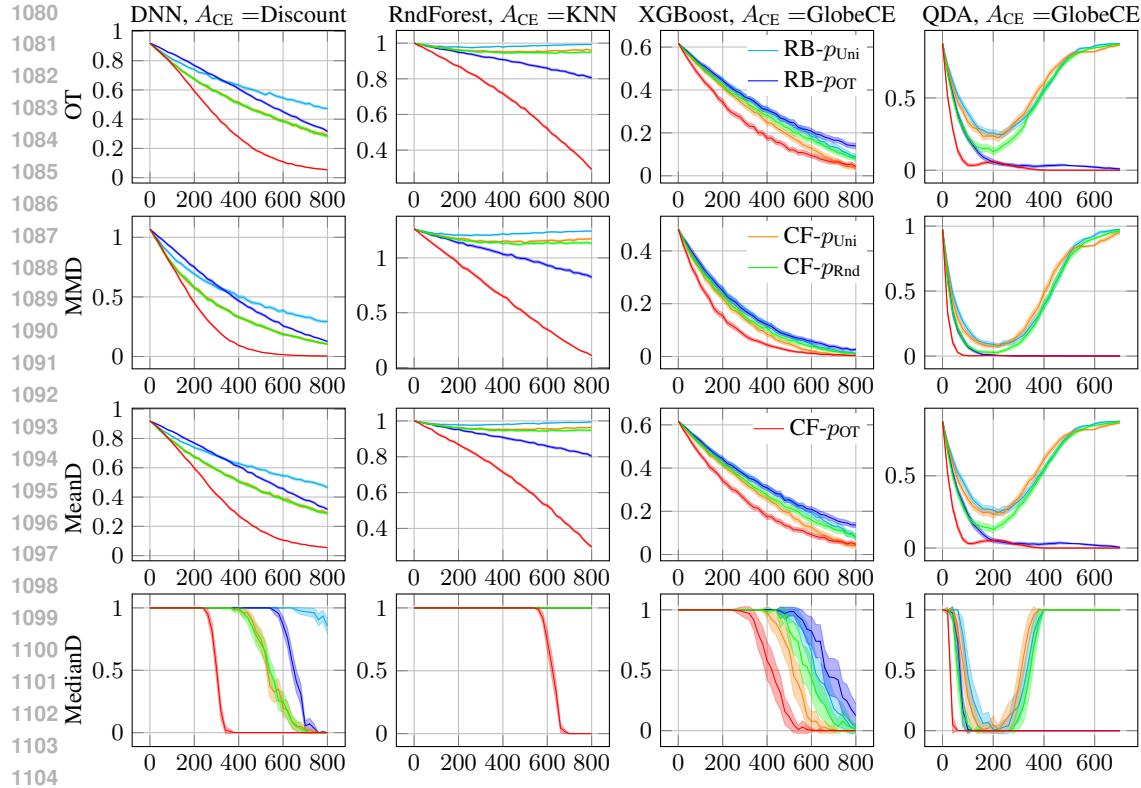


Figure 5: [HELOC] $D(f(\mathbf{z}), \mathbf{y}^*)$ vs. allowed actions C . Experiments are with 100 runs. The shadows show the 99.9% confidence intervals. The legends apply to all plots. $A_{\text{Value}}^{\text{avg}}$ is used.

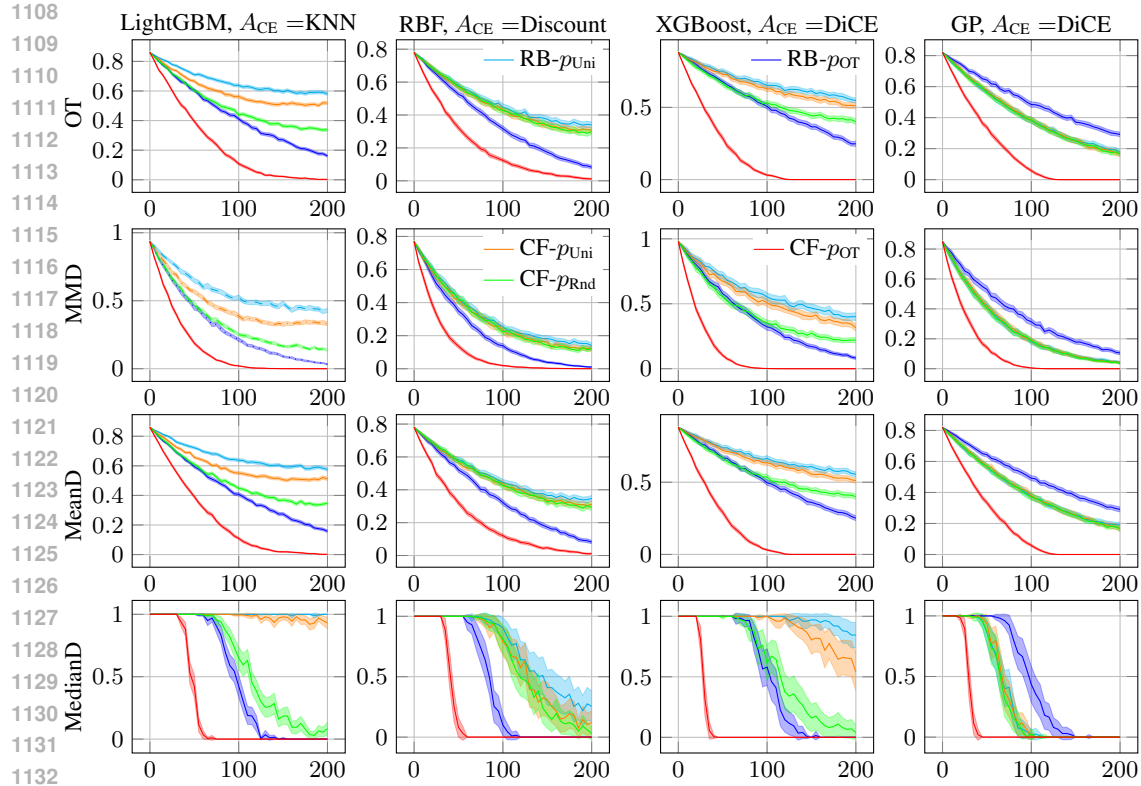
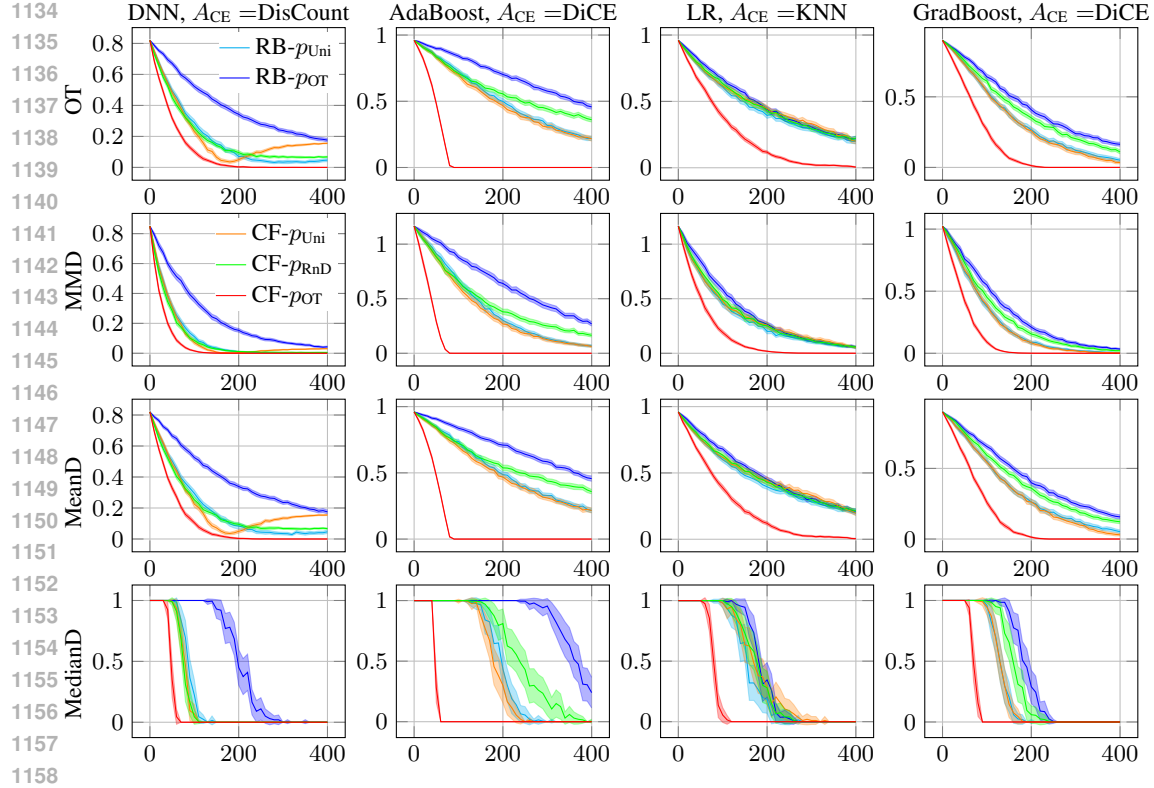
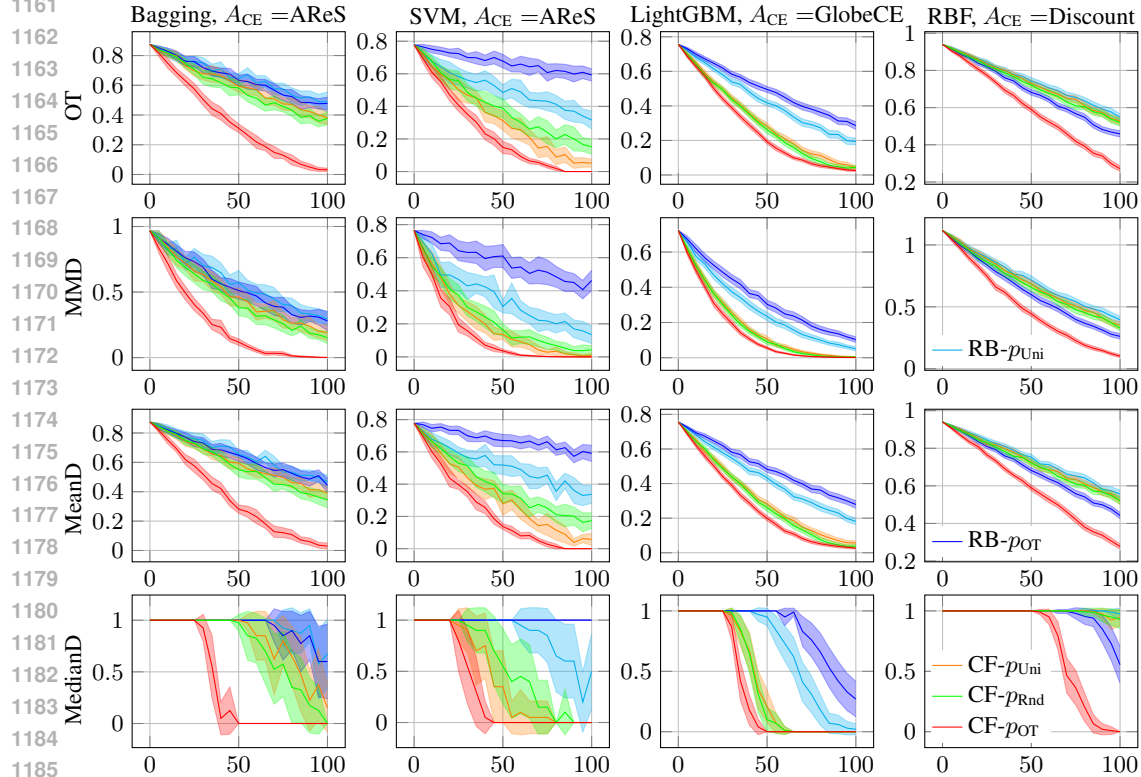


Figure 6: [German Credit] $D(f(\mathbf{z}), \mathbf{y}^*)$ vs. allowed actions C . Experiments are with 100 runs. The shadows show the 99.9% confidence intervals. The legends apply to all plots. $A_{\text{Value}}^{\text{avg}}$ is used.



1159 Figure 7: [Hotel Bookings] $D(f(\mathbf{z}), \mathbf{y}^*)$ vs. allowed actions C . Experiments are with 100 runs. The
 1160 shadows show the 99.9% confidence intervals. The legends apply to all plots. A_{Value}^{\max} is used.



1187 Figure 8: [COMPAS] $D(f(\mathbf{z}), \mathbf{y}^*)$ vs. allowed actions C . Experiments are with 100 runs. The
 1188 shadows show the 99.9% confidence intervals. The legends apply to all plots. A_{Value}^{\max} is used.